Normalization and Calibration of Geostationary Satellite Radiances for the International Satellite Cloud Climatology Project

YVES DESORMEAUX
Centre de Météorologie Spatiale, Lannion, France

WILLIAM B. ROSSOW
NASA Goddard Institute for Space Studies, New York, New York

CHRISTOPHER L. BREST
Hughes STX Corporation, NASA Goddard Institute for Space Studies, New York, New York

G. GARRETT CAMPBELL
Cooperative Institute for Research in the Atmosphere (CIRA), Colorado State University, Fort Collins, Colorado

(Manuscript received 30 October 1991, in final form 27 August 1992)

ABSTRACT

Procedures are described for normalizing the radiometric calibration of image radiances obtained from the suite of geostationary weather satellites that contributed data to the International Satellite Cloud Climatology Project. The key step is comparison of coincident and collocated measurements made by each satellite and the concurrent Advanced Very High Resolution Radiometer (AVHRR) on the "afternoon" *NOAA* polar-orbiting weather satellite at the same viewing geometry. The results of this comparison allow transfer of the AVHRR absolute calibration, which has been established over the whole series, to the radiometers on the geostationary satellites. Results are given for *Meteosat2, Meteosat3*, and *Meteosat4*, for *GOES5, GOES6,* and *GOES7*, for *GMS2, GMS3,* and *GMS4* and for *Insat-1B.* The relative stability of the calibrations of these radiance data is estimated to be within ±3%; the uncertainty of the absolute calibrations is estimated to be less than 10%. The remaining uncertainties are at least two times smaller than for the original radiance data.

1. Introduction

The International Satellite Cloud Climatology Project (ISCCP) began the collection and analysis of weather satellite imaging radiometer data in July 1983 to provide radiance and cloud datasets for climate research (Schiffer and Rossow 1983). A key goal is to provide globally uniform information over a long time period to explore the variations of clouds over a complete range of space and time scales (Schiffer and Rossow 1985). The primary focus of the analysis is to describe those physical properties of clouds that are most important for determining their effect on radiation; however, these same results may also elucidate the role of clouds in the hydrological cycle (Rossow and Schiffer 1991). In order to cover all scales of cloud variation from diurnal to interannual and from mesoscale to planetary, imaging data must be obtained from a combination of geostationary and polar orbiting satellites. The only common spectral channels available from the weather satellites are at a "visible" wavelength (VIS ≈ 0.6 μm) and a "window infrared" wavelength (IR ≈ 11 μm). To keep data volumes manageable, these images are sampled at 30-km and 3-h intervals.

To measure variations of cloud physical properties over long time periods, the radiance measurements obtained from all of these satellites have to be calibrated consistently. In particular, measurements from several satellites in a series, as well as from several different satellites, must be normalized to a single standard. Such a relative calibration standard is sufficient for study of changes, but an absolute calibration is required to determine the physical attributes of clouds from their effect on the measured radiances. Since the polar-orbiting satellites operated by *NOAA* underfly all of the geostationary satellites, the radiances obtained from the Advanced Very High Resolution Radiometers (AVHRRs) are used as the relative calibration standard

Corresponding author address: Dr. William Rossow, NASA Goddard Institute for Space Studies, 2880 Broadway, New York, NY 10025.

for all of the data. Intercalibration among the polar-orbiting satellites, corrections for their calibration drift in time, and an absolute calibration are described in Brest and Rossow (1992).

This paper concerns the normalization of the geostationary satellite measurements to those by AVHRR, which is done in two steps. The first step is to compare the geostationary radiances to those measured by the current "afternoon" polar orbiter at the same time and location with the same viewing geometry. Obtaining accurate normalization from this comparison requires careful selection of coincident images and detailed analysis to identify common targets. Thus, to limit the magnitude of the task the normalization data are comprised of four to five image samples per month. The comparisons are routinely performed every three months (January, April, July and October) by the ISCCP Satellite Calibration Center (SCC) at the Centre de Météorologie Spatiale (CMS) in Lannion, France; but they can be performed approximately every week, if needed, when satellites are changed or any unusual events occur. This normalization procedure accounts for "slow" drifts in the calibration of the geostationary satellite radiometers, where "slow" is defined by a time scale of about 1 3 months in practice. Section 2 describes this procedure for all of the geostationary satellites, except *Insat*. Because the special images, coincident with polar-orbiter observations, were not collected for *Insat*, a special procedure is performed for *Insat* radiances (Section 3) by the ISCCP Sector Processing Center (SPC) at Colorado State University (CSU) in Fort Collins, Colorado.

Changes in the calibrations also occur on shorter time scales, even between images. The second step of the calibration, performed at the ISCCP Global Processing Center (GPC) at NASA Goddard Institute for Space Studies (GISS) in New York, New York, is to examine the time history of the distribution of radiances in each image to locate sudden, systematic changes that exceed some minimum magnitude. Small additive factors are used to remove these changes. This procedure is described in Section 4.

The final calibration results are reported on the ISCCP Stage B3 data tapes in three stages: nominal, normalized and absolute. The nominal calibration is the best available information obtained from the satellite operator or the literature, usually the prelaunch calibration for the VIS channel and on-board calibration target results for the IR channel (Rossow et al. 1987). The nominal calibrations for each satellite are defined in an Appendix. The normalized calibration reports the results of the comparison with the current afternoon polar-orbiter measurements without regard to variations in the calibration of the polar orbiter, itself. Finally, the absolute calibration accounts for any short-term changes that are found and for any changes in the calibration of the polar-orbiter radiances. The absolute calibration tables on the Stage B3 data tapes represent the best calibration for each satellite.

Since production of stage B3 data began before a final calibration for the VIS channel of AVHRR (channel 1) was available, the absolute calibration was assumed to be that of the *NOAA-7* AVHRR in July 1983. Subsequent comparisons to aircraft flights over White Sands, New Mexico, showed this calibration to be 20% too low; thus, all VIS radiances on stage B3 data must be multiplied by a factor of 1.2 to obtain the final calibration (Brest and Rossow 1992).

Estimates of the calibration error are discussed and summarized in Section 5. Complete details of the calibration history of these radiometers can be obtained in a technical report (Rossow et al. 1992) that accompanies a digital dataset that is archived with the other ISCCP datasets[1]. The digital dataset contains the calibration tables for use with individual stage B3 images; refinements of the ISCCP calibration will be "published" by producing a complete new version of this dataset.

2. Normalization procedure

The radiance normalization procedure has six steps: 1) image selection, 2) data quality checks, 3) image preprocessing, 4) mapping and registration, 5) target selection, and 6) calculation of the normalization coefficients (called BC data).

The selected radiance data (called AC data) are portions of full-resolution images (pixel sizes range from 1 to 4 km in VIS and from 4 to 11 km in IR) obtained about four to five times per month. The analysis is routinely performed every three months (January, April, July and October); however, when a satellite is changed or if other information warrants it, the analysis can be done every month, or for individual images, separated by about one week. (The choices of four to five image samples per month and routine comparisons every three months were determined by practical limits on cost and manpower, but were considered frequent enough based on available experience. With the exception of spurious diurnal variations of IR calibration, which are discussed in section 4b, this frequency has proved sufficient.)

Some *Insat* radiance data have also been collected for ISCCP; however, no AC data were collected at the same time. Therefore, normalization of these radiances is performed by comparing overlapping observations between *Insat* and the normalized measurements from *Meteosat* and *GMS*. This procedure is described in section 3.

[1] The dataset is available from the Satellite Data Services Division, National Environmental Satellite Data and Information Service, National Oceanic and Atmospheric Administration, Princeton Executive Square, Room 100, Washington, D.C. 20233 (Telephone: 301-763-8400; FAX: 301-763-8443).

a. Overview

Since the spectral responses of the various satellite radiometers differ somewhat (the *Meteosat* "visible" channel differs most), the normalization procedure uses only clear ocean and clouds over ocean as targets (bright clouds over land are sometimes used) since the wavelength dependence of sunlight reflected from such scenes is more nearly that of the solar spectrum over a wavelength range of 0.45-0.95 μm. Thus, the interpretation of these calibrations is that they represent the instrument response to radiation with a spectral distribution the same as the sun for VIS and the same as a blackbody for IR (Rossow et al. 1987). While this approach provides a standardized measure of the total amount of energy that the radiometer receives, it does not provide a completely accurate representation of the nature of the radiation measured when the spectrum is strongly changed by the target.

To minimize the spectral dependence of the radiances, the VIS radiances are converted into scaled radiances (the measured radiance divided by the instrument's "solar constant"),[2] and the IR radiances are converted into brightness temperatures (see the Appendix and Rossow et al. 1987). Although the linearity of the responses of the various radiometers is not the same, the normalization procedure assumes a linear relation among the scaled radiances and brightness temperatures from the several satellites. This linearity is shown to be approximately correct for all cases.

Cloudy radiances generally exhibit significant variations at both small spatial and temporal scales, although at scales less than 100 km and 1 h the magnitude of these variations is generally smaller than at larger scales (Sèze and Rossow 1991). To minimize the effects of could changes, strict criteria for the simultaneity and collocation of the measurements are applied, radiances are taken from small targets about 50 km × 50 km in size, only cloud targets that exhibit narrow (about ±7% in VIS and ±7 K in IR) radiance distributions are used, and the more radiance value, rather than the average radiance value, is used to reduce effects of image navigation errors. The normalization coefficients are then determined from a linear regression of greater than 50 pairs of radiances distributed over the observed range.

b. Image sector Selection

1) SELECTION OF SECTOR LOCATIONS

Since the satellite zenith angle varies much more rapidly over a region when viewed from the lower-altitude polar orbiter than from the geostationary satellites, polar-orbiter swaths passing near the geostationary subsatellite point (near the equator) will always include a region of similar viewing geometry. About five image sectors[3] per month are collected from full resolution geostationary images, representing an area about 2000 km on a side (about 20° of latitude/longitude) and centered on the subsatellite point. To obtain the best normalization of the radiances, the selected sectors should contain radiances covering as large a range of values as possible; however, the proper kind of clouds (bright and cold usually associated with large, deep convective storm complexes) are not always found near the geostationary subsatellite points.

The *Meteosat* subsatellite point (0°, 0°)[4] is an ocean location in the Gulf of Guinea. A major area of deep convection near this location moves seasonally from the gulf in winter (boreal seasons will be used throughout) into northern Africa in summer. The region south of the equator is always dominated by the St. Helen anticyclone, where there are very few deep convective events. Sometimes in summer, little convection is present over the oceans in the image near (0°, 0°), so that deep convective clouds over land must be used.

The *GMS* subsatellite point (0°, 140°) is an ocean location just north of Papua New Guinea. This region of the western tropical Pacific is dominated by frequent deep convection at all times of the year, giving normalization results superior to all other satellites. However, *GMS* operations do not produce images every 30 min like the other geostationary satellites; instead, images are collected with a variable time separation from 30 min to 3 h over the diurnal cycle. Thus, image sectors must be selected east or west of the subsatellite longitude to be coincident with the polar-orbiter time. For example, the nominal overflight time of *NOAA-7* and *NOAA-9* is about 0545 UTC, but this time changes over the lifetime of the polar orbiters. Thus, in February 1985, an image sector was selected at (0°, 156°) to coincide with the overflight of *NOAA-7*, which was at the end of its operational lifetime. To coincide with *NOAA-9*, at the beginning of its operation, in February 1985, the image sector was located at (0°, 129°); but by October 1988 at the end of the *NOAA-9* operations, the sector had moved back to (0°, 156°). Since *NOAA-11* enters the *GMS* areas at 0430 UTC, collection of special image sectors by the Japan Meteorological Agency (JMA) was required to obtain simultaneous data.

The *GOES* East subsatellite point (0°, 285°) is a land location at the juncture of the borders of Ecuador, Colombia and Peru. To the west over the Pacific, there

[2] This quantity, when divided by the cosine of the solar zenith angle, is a reflectance that may be the function of viewing and illumination geometry. Both the scaled radiance and the reflectance are very frequently, and mistakenly, called albedo.

[3] We will use the terms *image sector* or *sector* to refer to a portion of a satellite image covering a particular geographic location.

[4] All location in this paper will be given as (latitude, longitude) in degrees from the equator (±90°) and eastward from the Greenwich meridian (0°-360°).

is a permanent anticyclone region with stratocumulus and broken cumulus clouds that do not provide either very bright or very cold targets. However, to the northwest there are deep convective clouds over the ocean, especially in summer; also some deep convection occurs over land to the northeast. In winter the Amazon lowlands are covered by deep convective clouds that can be used for the brightest and coldest targets.

The *GOES* West subsatellite point (0°, 225°) is an ocean location in the eastern Pacific. The intertropical convergence zone (ITCZ) in this area is permanently located at about 10° N, just at the edge of the image sector centered on the subsatellite point. In some seasons, the frequency of deep convective events is very low within the sector. Thus, normalization using images from the subsatellite point was difficult because few bright (cold) clouds were available. The area for *GOES* West image sectors was shifted northward to find better cloudy radiances; however, this introduces larger differences in satellite viewing geometry between the polar orbiter and *GOES* West. After trying a "dynamic" scheme, where the images were examined every month to find acceptable radiance ranges before sector selection, the final location of *GOES* West AC image sectors was chosen to be at (5°, 225°).

At the end of July 1984, *GOES-5* (EAST) failed and was not replaced until April 1987 (by *GOES-7*). At the end of January 1989, *GOES-6* (WEST) failed and has not yet been replaced. Consequently, over the first eight years of ISCCP data collection, two *GOES* satellites were available only about 36% of the time. During operations of a single *GOES* satellite (called *GOES* Center), its subsatellite point (0°, 252°-262°) is an ocean location west of the Galapagos islands. Although the ITCZ in this area is generally more active, its location is always near 10° N, so the AC image sectors are selected to be at (5°, 252°-262°).

2) Criterion for coincidence

On the 15th day of every month, all coincidences in the following month between each geostationary satellite and the "afternoon" polar orbiter are found, based on the orbital predictions for the polar-orbiter equator crossing times and the subsatellite latitudes and longitudes, and the imaging schedules for the geostationary satellites. Image time for the geostationary satellites is the time when the image center is scanned, determined from the scheduled beginning of the image and the approximate scan-line number at the image center. Of all the predicted coincidences that meet the minimum requirements of a time difference less than 10 min and a polar-orbiter nadir track within 500 km of the subsatellite (or other selected) point, the five are selected to minimize the time and distance differences. These image sectors are then requested from each of the ISCCP SPCs (European Space Agency for *Meteosat*, Canadian Atmospheric Environment Service for *GOES* East, Colorado State University for *GOES* West, Japan Meteorological Agency for *GMS*, and *NOAA* for the polar orbiters).

3) Quality checks and preprocessing

Upon receipt of AC datasets from the SPCs, simple quality checks are made to be sure that there are no errors on the data tapes and that the radiance data are from the proper images and have been successfully transcribed. The radiance data are in the form of instrument counts. These are converted to radiances by application of the nominal calibration obtained from the satellite operator or from the literature (see definitions in the Appendix and Rossow et al. 1987). Visible radiances are expressed as reflectances (scaled radiances divided by the cosine of the solar zenith angle) with a precision of 0.5%, and IR radiances are expressed as brightness temperatures with a precision of 0.5 K. The higher spatial resolution visible measurements are averaged to the lower resolution of the IR measurements.

4) Mapping and registration

All AC data, whether from polar or geostationary satellites, are reprojected into an equal-angle map grid centered on the selected center coordinates, defined above. The map resolution is about 3 km covering a region of about 15° of latitude and longitude. Mapping is performed by a "nearest neighbor" technique; that is, the radiance value placed in the target map cell comes from the image pixel with latitude-longitude values nearest the center coordinates of target map cell. Since the map resolution is slightly higher than the highest-resolution satellite image, this causes some replication of the radiance values.

The mapped pairs of polar orbiter and geostationary images are compared to remove residual differences in location caused by navigation errors. Image registration is determined by shifting the relative coordinates by ±9 increments and calculating the sum of the absolute differences of radiances from the two satellites in five test subareas. The best registration is the shift that minimizes the sum. The typical magnitude of the calculated shifts has been less than three map cells (i.e., navigation differences are less than 10 km); however, occasionally the shifts are two to three times larger. Synthetic tests of the normalization method show that offsets larger than one map cell reduce the accuracy of the results, so this step is important to the accuracy of the results.

c. Selection of radiance samples

The area covered by both the polar-orbiter and geostationary satellites is automatically divided into square regions of 14 pixels × 14 lines, called targets,

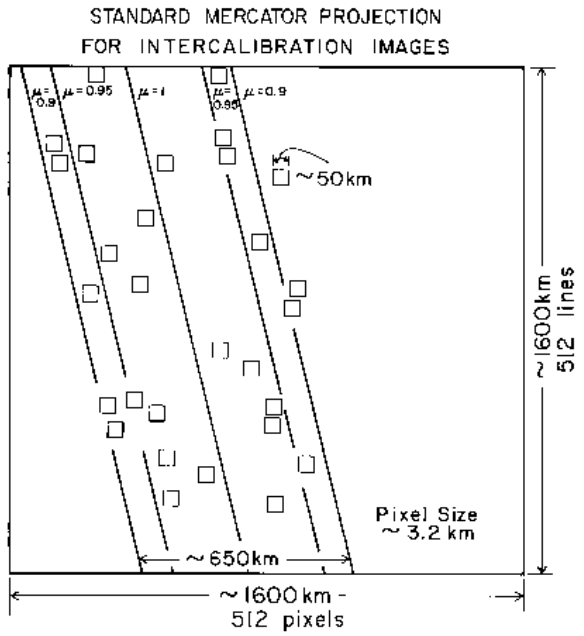

FIG. 1. Illustration of viewing geometry constraints on selection of radiance targets from polar-orbiter data near the geostationary subsatellite point. The lines indicate values of the polar satellite viewing zenith angle (cosine of this angle is μ). Typical targets, composed of 14 x 14 map cells, are shown as small squares.

for comparison of their radiances. These targets are tested against four criteria: 1) the time difference between the images is less than 10 min (which also insures a similar cosine of the solar zenith angle μ_0 within ±0.01-0.04), 2) the target locations are the same (within plus or minus one map cell), 3) the cosine of the satellite zenith angles μ is the same to within 0.05 for VIS and 0.10 for IR, and 4) the radiance distribution within the target area is narrow, defined by a standard deviation less than 7% in VIS and 7 K in IR. The first and second criteria are met by image sector choice and the registration of mapped images. All targets that do not meet these criteria are discarded.

For cases where the geostationary satellite image sectors are near the subsatellite point, the value of μ is everywhere greater than 0.9, so the search area for targets is limited to the portion of the polar-orbiter image sector where μ > 0.95 for VIS and 0.9 for IR (Figure 1). Since the azimuthal dependence of the scattered VIS radiation is weak for μ > 0.9, no relative azimuth[5] constrain is applied. For cases where the geostationary satellite image sector is located away from the subsatellite point, both images are searched to identify regions with similar μ values. In addition, for VIS radiance comparisons, the relative azimuth angle is constrained to be less than or equal to 60° when the difference in $\mu \leq 0.02$, and to be less than or equal to 20° when the difference in μ is greater than 0.02 but less than 0.05 (Fig. 2). The specular reflection regime is also removed from the VIS comparison by requiring that $|\mu - \mu_0| > 0.05$.

Target testing continues to maximize the radiance range covered (typically about 0.85 in reflectance and 95 K in brightness temperature) and to obtain more than one sample in each of 30-40 radiance intervals in this range (radiance increments are 0.025 in reflectance and 2.5 K in bright ness temperature). A minimum of 50 targets is required. Usually these criteria are satisfied by processing three of five available image pairs; more than 80% of months processed meet target radiance distribution criteria. The most frequent radiance value (mode) and the standard deviation of the radiance distribution are determined from all targets that meet all criteria. The results of the target selection process are displayed to an operator superposed on the polar-orbiter image sector to check for and eliminate occasional image artifacts or problems caused by missing scan lines.

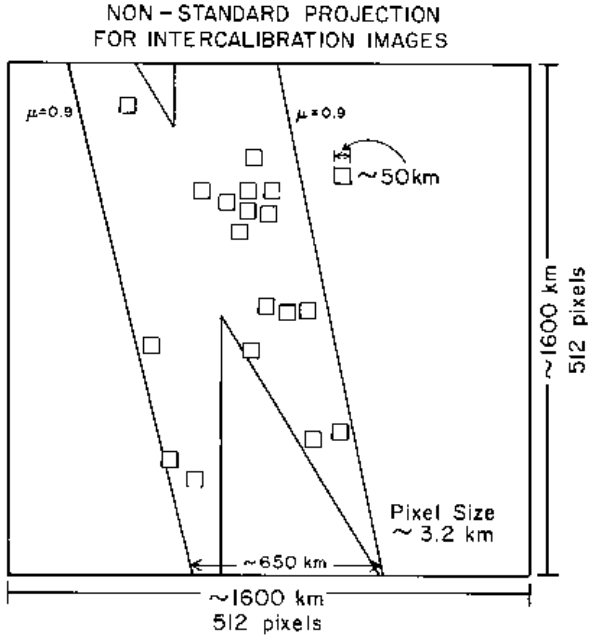

FIG. 2. Same as Fig. 1 but for polar-orbiter data that is 16° of longitude from the geostationary subsatellite point. Outer boundary is established by a limit on the polar satellite viewing zenith angle, and the inner boundaries are the result of constraints on the relative azimuth angle between the satellite view and solar illumination vectors.

[5] The relative azimuth angle is the angle between the plane containing the solar illumination vector and the local nadir direction and that containing the satellite view vector and the local nadir.

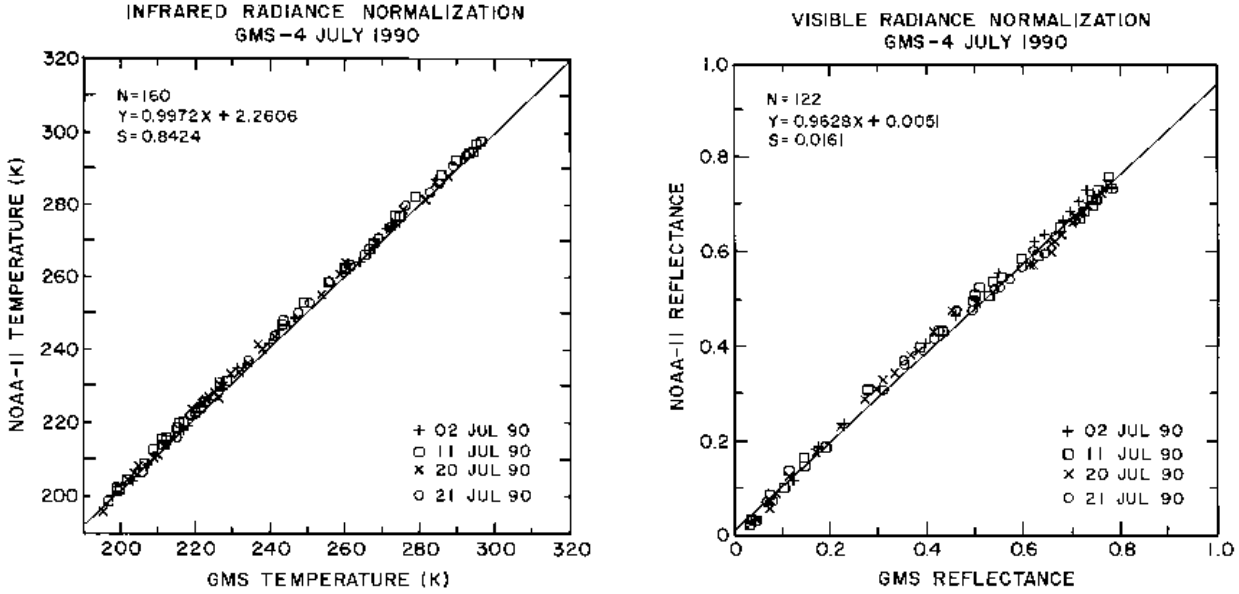

FIG. 3. Example os regresion plot of the mode of values of (a) infrared and (b) visible radiances for individual targets in four coincident *GMS-4* and *NOAA-11* images for July 1990. The best linear fit to these pairs of radiance values is shown: the equation is shown in the upper left, along with the number of targets, *N*, and their rms deviation from the line, *S*. Different symbols are data from different image pairs.

d. Normalization Coefficients

1) CALCULATION

All of the mode radiance values from targets in each geostationary-polar-orbiter satellite pair are considered to be the coordinates of a two-dimensional scatterplot (Fig. 3). A linear least-squares fit is calculated for each image pair and for all pairs combined; slope and intercept values are determined. Deviations of each target radiance from the geostationary data with respect to the combined regression fit are also determined (Fig. 4). The results for individual image pairs are examined for

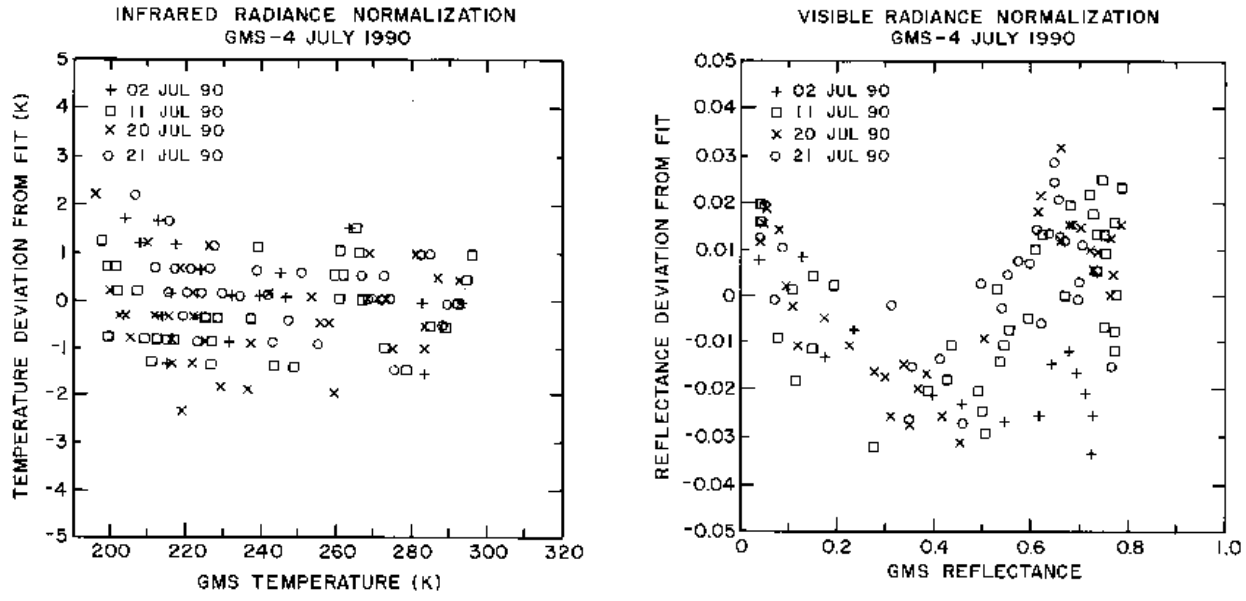

FIG. 4. Deviation of individual target mode radiances, (a) infrared and (b) visible, measured by *GMS-4* for July 1990 about the best linear fit shown in Fig. 3. Different symbols are from different image pairs.

evidence of shorter-term changes in radiometer performance by comparing the mean deviation from each pair to the average deviation of all pairs. If mean deviations of individual pairs are smaller than the average over all pairs, then the combined slope and intercept values are reported for that month; if not, the analysis is performed for more image sector pairs in that month and/or for preceding and following months to isolate the change and obtain sufficient statistics for the normalization before and after the change. Typical values of the rms deviations from the regression fit are 1%-2% for VIS and 1-2 K for IR.

If there are nonlinear differences in the radiometers, they will show as systematic variations of the differences over the full radiance range. Figure 4a shows the comparison of *GMS-4* and *NOAA-11* IR brightness temperatures; the fact that there is no systematic deviation of the brightness temperatures over the whole range from 200 to 300 K shows that use of a temperature scale for the normalization does not introduce any significant problem. In Fig. 4b, on the other hand, there is some evidence for a small (2%) difference in the linearity of the visible channels for these two satellites, as shown by the curvature of the target radiance deviations from a linear fit. Table 1 summarizes upper limits on nonlinearities found in this analysis for all satellites.

2) SENSITIVITY TEST

To determine the sensitivity of the normalization procedure to changes in radiometer calibration, selected datasets were reanalyzed after introduction of synthetic changes in the geostationary calibration, represented by gain changes of 1%, 5% and 10% (i.e., multiplying factors of 1.01 and 0.99, etc.), offsets of 1%, 5%, 10%, and all combinations of gain and offset changes. Table 2 illustrates some test results. Shown are the changes in the best linear fit slope and intercept values from the reference case produced by multiplying the *Meteosat* radiances by the factor indicated. These results show that the normalization procedure is sensitive to relative changes in calibration greater than 2%.

Table 1. Summary of upper limits on the magnitude of non-linear deviations about the mean for geostationary radiometers with respect to AVHRR determined from figure similar to Fig. 4. Visible deviations are in percent (scaled radiances) and infrared deviations are in Kelvins.

Geostationary satellite	Polar orbiter	Visible channel	Infrared channel
Meteosat-2	*NOAA-7*	--	0.5
Meteosat-2	*NOAA-9*	1.0	2.0
Meteosat-3	*NOAA-9*	1.5	1.5
Meteosat-3	*NOAA-11*	1.0	1.5
Meteosat-4	*NOAA-11*	1.0	1.0
GMS-1	*NOAA-7*	1.5	1.5
GMS-2	*NOAA-7*	1.5	1.5
GMS-3	*NOAA-7*	2.0	2.5
GMS-3	*NOAA-9*	2.0	2.0
GMS-3	*NOAA-11*	2.0	2.0
GMS-4	*NOAA-11*	2.0	2.0
GOES-5	*NOAA-7*	5.0	3.0
GOES-6	*NOAA-7*	2.0	1.5
GOES-6	*NOAA-9*	1.5	2.0
GOES-6	*NOAA-11*	1.5	1.0
GOES-7	*NOAA-9*	3.0	2.0
GOES-7	*NOAA-11*	2.0	1.0

TABLE 2. Changes in normalization slope and intercept, expressed as ratios, associated with synthetic changes of gain and offset introduced into AC data for *Meteosat*. The second part of the table shows one case where the synthetic changes are introduced into the polar orbiter data. The original slope (intercept) values are 1.013 (-2.6) for IR and 1.00 (-0.022) for VIS.

Multiplying factor	Change in IR		Change in VIS	
	Slope	Intercept	Slope	Intercept
0.90	1.112	14.8	1.115	0.95
0.95	1.053	7.6	1.051	0.91
0.99	1.010	2.3	1.013	1.00
1.00	1.000	1.0	1.000	1.00
1.01	0.990	-0.2	0.988	0.95
1.05	0.958	-4.8	0.952	1.00
1.10	0.908	-10.4	0.908	1.00
1.10	1.100	13.3	1.106	1.09

3) REPORTED STATISTICS

The final BC dataset produced by CMS and sent to GISS contains statistical results for each radiometer, separately: the best linear fit slope and intercept and the rms deviations with respect to the best fit line. In addition, the maximum, mean and minimum target mode radiances and the number and type of targets are reported. Summary information gives the date and time of each image pair used, the satellite name-number, and the spectral channel identifiers. Mode count and radiance values for each pair of satellites are also listed for each target, together with identifying information for the image data used, along with the figures like Figs. 3 and 4. All of this information is gathered for each spectral channel for each time period and sent to the ISCCP GPC.

e. Discussion of results

Figures 5 and 6 illustrate the history of the normalization of the geostationary radiometers by showing the changes made to two radiance values at the extremes of the full range for both the infrared and visible channels. For the infrared channel, the changes at 300 K and 200 K are shown (Figs. 5a and 5b, note the change of scale). The normalization coefficients are listed for each month in the Appendix; these values can be used directly to calibrate radiance data from these satellites.

The small systematic increase of all the geostation-

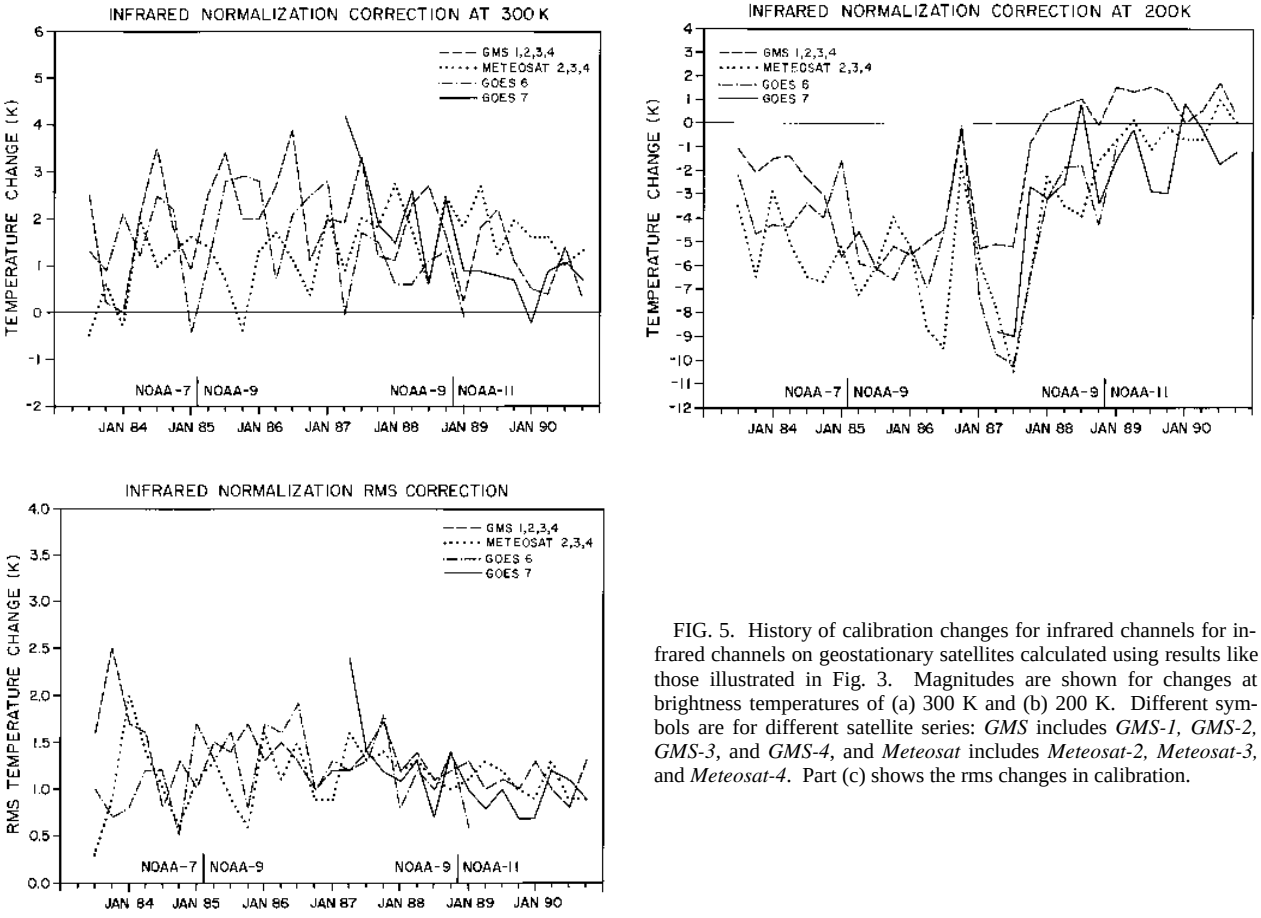

FIG. 5. History of calibration changes for infrared channels for infrared channels on geostationary satellites calculated using results like those illustrated in Fig. 3. Magnitudes are shown for changes at brightness temperatures of (a) 300 K and (b) 200 K. Different symbols are for different satellite series: *GMS* includes *GMS-1, GMS-2, GMS-3*, and *GMS-4*, and *Meteosat* includes *Meteosat-2, Meteosat-3,* and *Meteosat-4*. Part (c) shows the rms changes in calibration.

ary satellite calibrations for high temperature targets may be associated with the fact that the spectral response of the IR channel on the *NOAA* polar orbiters occurs at a slightly smaller wavelength than for all of the geosta tionary satellites; thus, the effects of water vapor absorption in the atmosphere would cause a small bias. The shorter-term variations show that the geostationary IR calibrations are more variable than that of the polar orbiter (cf, Brest and Rossow 1992), varying about ±1.01.5 K (Fig. 5c).

During the period from April 1985 - July 1988, when the same set of satellites were operational (*NOAA-9, Meteosat-2, GMS-3,* and *GOES-6),* significant variations occur; but the patterns for all geostationary satellites are quite similar (especially in Fig. 5b). These larger coordinated variations (in October 1986 and 1987) were caused by changes in the polar orbiter IR calibration procedure (Brest and Rossow 1992), rather than in the calibration of the geostationary satellites. This multi-satellite calibration comparison has proven very valuable in separating events occurring on one satellite from other sources of apparent variation.

The lack of any systematic change in IR normalizations between January and April 1985, when *NOAA-7* was replaced by *NOAA-9*, and between October 1988 and January 1989, when *NOAA-9* was replaced by *NOAA-11*, confirms the relative calibrations of these AVHRRs. Moreover, there is better agreement among the geostationary satellites of a particular series (i.e., *GOES*, *GMS* or *Meteosat*) than among the different series of satellite: compare *GOES-6* and *GOES-7* IR normalization, the transitions from *Meteosat-2* to *Meteosat-3* in July-October 1988 and from *Meteosat-3* to *Meteosat-4* in April-July 1989, and the transitions from *GMS-2* to *GMS-1* in January-April 1984, from *GMS-2* to *GMS-3* in July-October 1984, and from *GMS-3* to *GMS-4* in October 1989-January 1990. This illustrates the basic calibration stability of these radiometers, but the differences, which can be traced to different treatments of on-board calibration (cf. Rossow et al. 1987), show the need to normalize them to a common standard. Note also that, since the relationship between measured radiant energy and brightness temperature is very nonlinear, the larger temperature deviations at colder temperatures actually represent about the same amount of energy as the smaller deviations at warmer temperatures.

Specific events that appear in Fig. 5 for particular satellites that have been independently confirmed: 1) *Meteosat-2* underwent a rapid drift in gain from mid-1986 until it was replaced by *Meteosat-3* in mid 1988, which was not entirely compensated by the ESA cali-

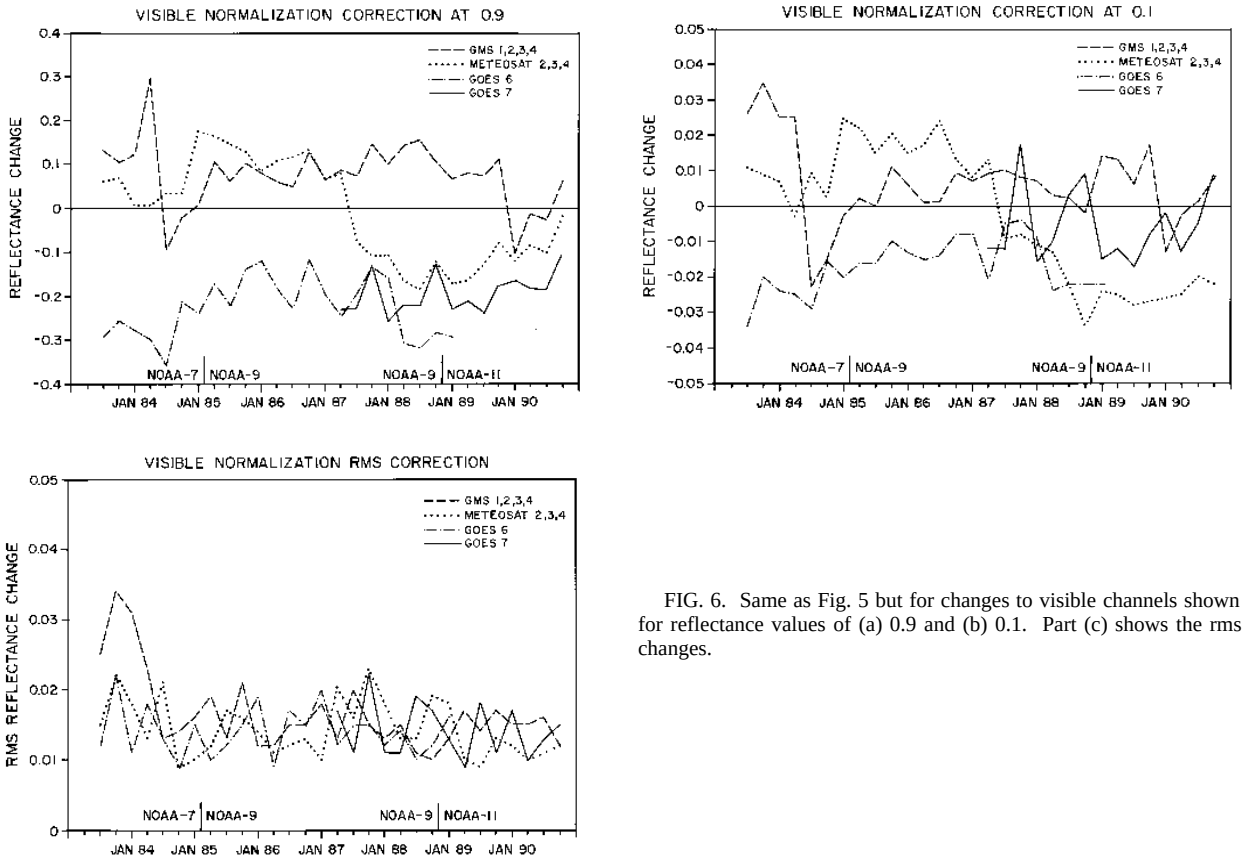

FIG. 6. Same as Fig. 5 but for changes to visible channels shown for reflectance values of (a) 0.9 and (b) 0.1. Part (c) shows the rms changes.

bration procedure; 2) *GOES-6* IR calibration is generally more variable than that of the other satellites (see section 4).

Figure 6 shows similar results for the visible channel, illustrated by the changes at 10% and 90% reflectance (note the change in scale); Fig. 6c shows the rms changes. Very small, but systematic, changes are discernable at the times of transition between different *NOAA* polar orbiters (January-April 1985, October 1988 -January 1989), consistent with small differences in the VIS calibration for the polar orbiters (Brest and Rossow 1992). A trend in the *GMS* and *GOES* normalizations through the period from January 1985 to October 1988 is associated with the drift of the *NOAA-9* calibration (Brest and Rossow 1992). At the same time, *Meteosat-2* is drifting more rapidly in the other direction, which finally required a 20% gain change by ESA on 12 May 1987; a sudden change in the normalization appears at the same time in Fig. 6. The differences of VIS calibrations among the different satellites series are much larger than the relative variations for each satellite over the first few years; but after the *Meteosat* gain change and the transition from *GMS-3* to *GMS-4* (October 1989-January 1990), all three geostationary satellites appear to have more similar visible channel calibrations.

Differences between satellites of the same series are also apparent in both Figs. 6a and 6b and illustrate the need for normalization to a common standard: for example, the transitions between *GMS-2* and ***G**MS-1* (January-April 1984), between *GMS-2* and *GMS-3* (April -July 1984), and between *GMS-3* and *GMS-4* (October 1989-January 1990) are readily apparent. The VIS calibrations between satellites of the *Meteosat* and *GOES* series seem more similar. The relative stability of the VIS channels of all these radiometers seems high, with rms changes of only about 2% required (Fig. 6c).

3. Normalization of *Insat* radiances

Since no AC data were collected for *Insat*, a different method is used by CSU to normalize *Insat* radiances to the same standard as the other satellites. In this case, the *Insat* data, sampled to a spacing of about 25 km, are compared to overlapping stage B3 data from *Meteosat* and *GMS,* mostly over areas in the southern Indian ocean to avoid strong effects due to differences in the spectral responses of the radiometers. The *Meteosat* and *GMS* radiances are first adjusted to the polar-orbiter radiances, as described in section 2. The *Insat*

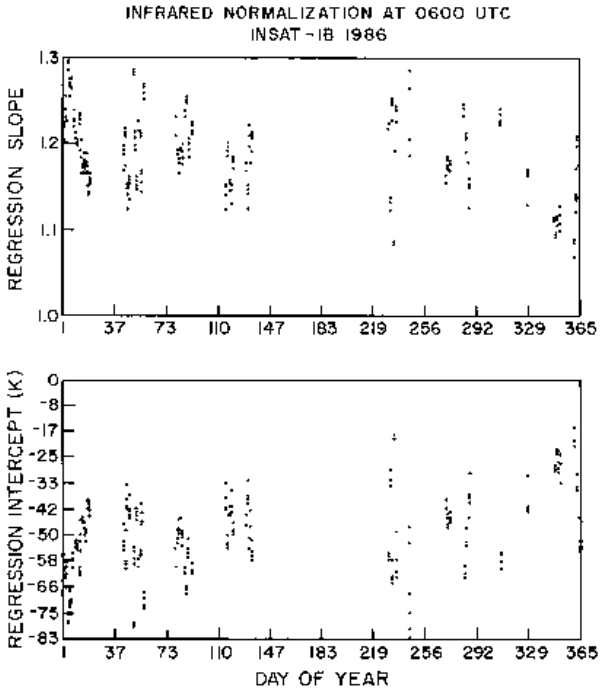

FIG. 7. History of calculated slope and intercept coefficients for infrared radiances from Insat-1B compared with normalized GMS-3 for 1986. Comparison images collected near 0600 UTC.

normalization method is, in fact, the method originally proposed for normalizing the geostationary satellite data for ISCCP; however, the normalization to a single polar-orbiting satellite was preferred because the simultaneity and viewing-geometry constraints can be made much stronger.

The sampled images from *Insat*, *GMS* and *Meteosat* are collected at the same *nominal* time and remapped to a common cylindrical equidistant grid at 1/3° resolution. (For the first two years of *Insat* data, 1986-87, images were supplied only two times per day, 0600 and 1200 UTC; for April 1988-March 1989 images were supplied eight times per day.) The radiances in individual map cells for several regions and each satellite pairing become coordinates of points in a two-dimensional scatterplot. Since time differences between *Insat* and either *Meteosat* or *GMS* images can be as large as 15-45 min, more data have to be compared to compensate for variations associated with cloud changes. Moreover, earth-location uncertainties are larger than the image pixel sizes, which introduces additional differences. To minimize these effects, four variance thresholds are applied to each region to identify more homogeneous scenes for the radiance comparisons. The results were found to be nearly independent of the threshold value, indicating that a statistically stable result has been obtained. The final results represent an average over all variance thresholds.

Variations of the slope and intercept values derived for individual days, scattered over the first year of *Insat* data, are illustrated in Fig. 7 for the *GMS* comparison at 0600 UTC (these results are typical of those for the remaining years). Four points are shown for each day, representing different regions in the images. There is no obvious trend to these results over this time period; however, the scatter of values is relatively large (about ±5% in slope and ±15 K in intercept). In 1988 a small trend over the year is apparent for infrared radiances (not shown); however, use of the annual mean adjustment has about the same effect on the distribution of *Insat* radiance as application of adjustment values from individual days. The variations of the infrared slope and intercept values nearly cancel each other for temperatures between 200 and 300 K. Similar results were obtained for VIS radiances. The recom-

TABLE 3. Annual summary of normalization slope (intercept) for Insat radiances when compared to *GMS* and *Meteosat* radiances for 1986-1988. Recommended values are marked by the asterisk. The nominal calibration for Insat is described in the Appendix.

Year	Comparison Satellite		Visible		Infrared	
			Slope	Intercept	Slope	Intercept
1986	GMS	0600 UTC	1.008	(+0.018)	1.187	(-50.7 K)*
	GMS	1200 UTC	—		1.209	(-55.4 K)
	Meteosat	0600 UTC	—		1.177	(-50.6 K)
	Meteosat	1200 UTC	—		1.191	(-53.4 K)
1987	GMS	0600 UTC	1.003	(+0.022)	1.193	(-48.8 K)*
	GMS	1200 UTC	—		1.219	(-55.5 K)
	Meteosat	0600 UTC	—		1.149	(-41.3 K)
	Meteosat	0600 UTC	—		1.179	(-48.6 K)
1988	GMS	0600 UTC	1.058	(+0.000)	1.109	(-28.3 K)*
	GMS	1200 UTC	—		1.129	(-34.0 K)
	Meteosat	0600 UTC	—		1.125	(-35.6 K)
	Meteosat	1200 UTC	—		1.146	(-41.5 K)

mended normalization of *Insat* for 1986-88 is that obtained by comparisons to *GMS* radiances at 0600 UTC, given in Table 3.

Results for 1988 show some significant changes in the IR calibration; calibration values supplied by the Indian Meteorological Department also exhibit some variations, but these results were not used. (Several images in March 1988 also appear to have anomalous calibrations, associated with shadowing of the satellite during eclipse of the sun by the Earth.) Results for April 1988 give a slope and intercept of 1.040 and -11.0 K for IR radiances. No spurious diurnal cycle in calibration is apparent.

4. Fine adjustment procedure

The normalization procedures described in the previous two sections are designed to correct for relatively slow changes (time scale of order one month) in the calibration of the geostationary satellite radiometers, although occasional abrupt changes are also corrected. In this section, we describe an additional procedure that is applied to all of the satellite data, including the polar-orbiter data, to correct for any short-term changes in calibration. In practice, "short means on time scales from 3 h to 1 month.

a. Radiance statistics

1) EXAMPLES OF RADIANCE VARIATIONS

The basic method for finding short-term changes is to examine 2-week records of the radiance distribution for each whole image, represented by the mean value, plus and minus one standard deviation, together with the 10th, 25th, 50th, 75th and 90th percentile values. Figures 8 and 14 show examples of 2-week periods of typical infrared and visible data. The lower percentile values, separated into land and water positions, represent low VIS radiances and high IR temperatures, respectively. These examples illustrate the statistical stability of the radiance distributions from image to image when taken over large water-covered portions of the earth. The darker VIS and warmer IR statistics are controlled by clear regions in the tropics (if the image is limited solely to the tropics, there is no change in the

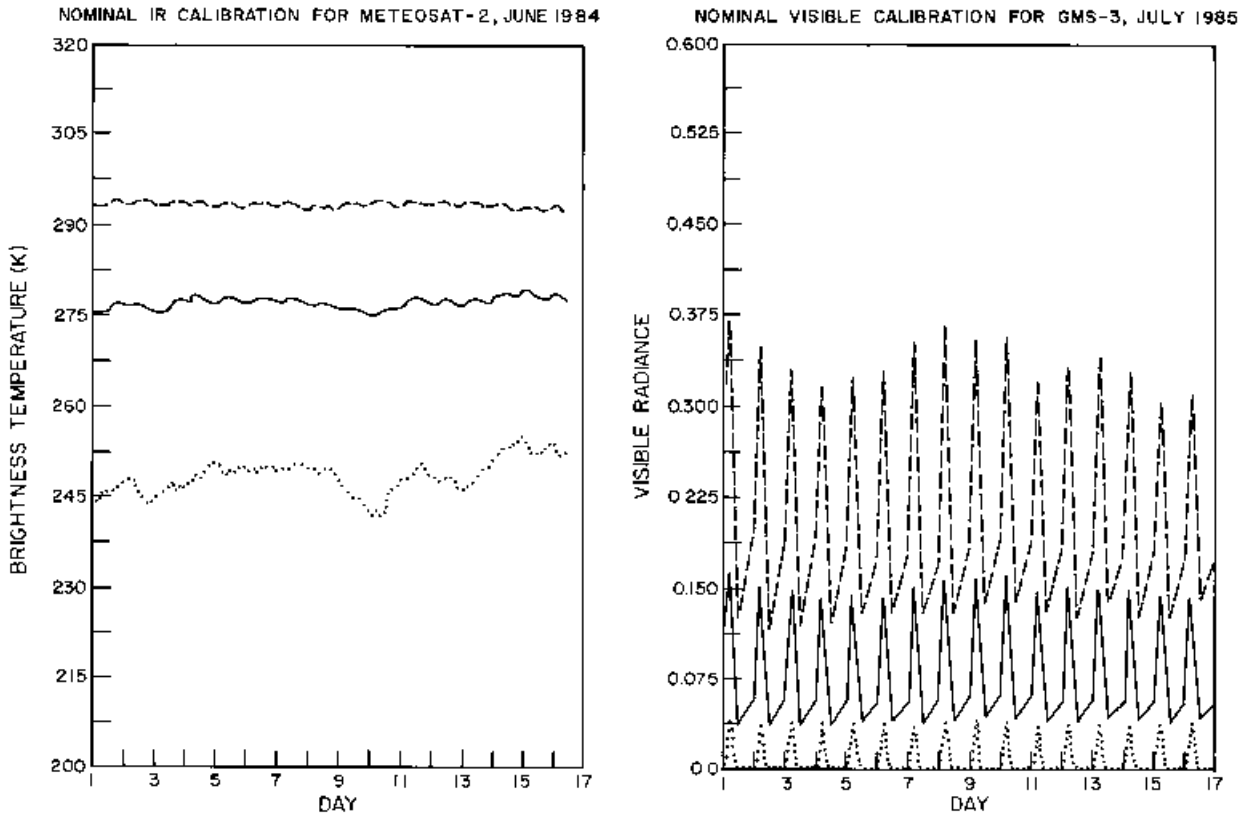

FIG. 8. History of the mean value (solid) and the 10th (dashed) and 90th (dotted) percentile values from the distribution of radiances over water for individual images for a 16-day period from (a) *Meteosat-2* from 1 to 16 June 1984 for infrared and from (b) *GMS-3* from 1 to 16 July 1985 for visible. The large, regular variations of VIS radiances are caused by diurnal variations of illumination.

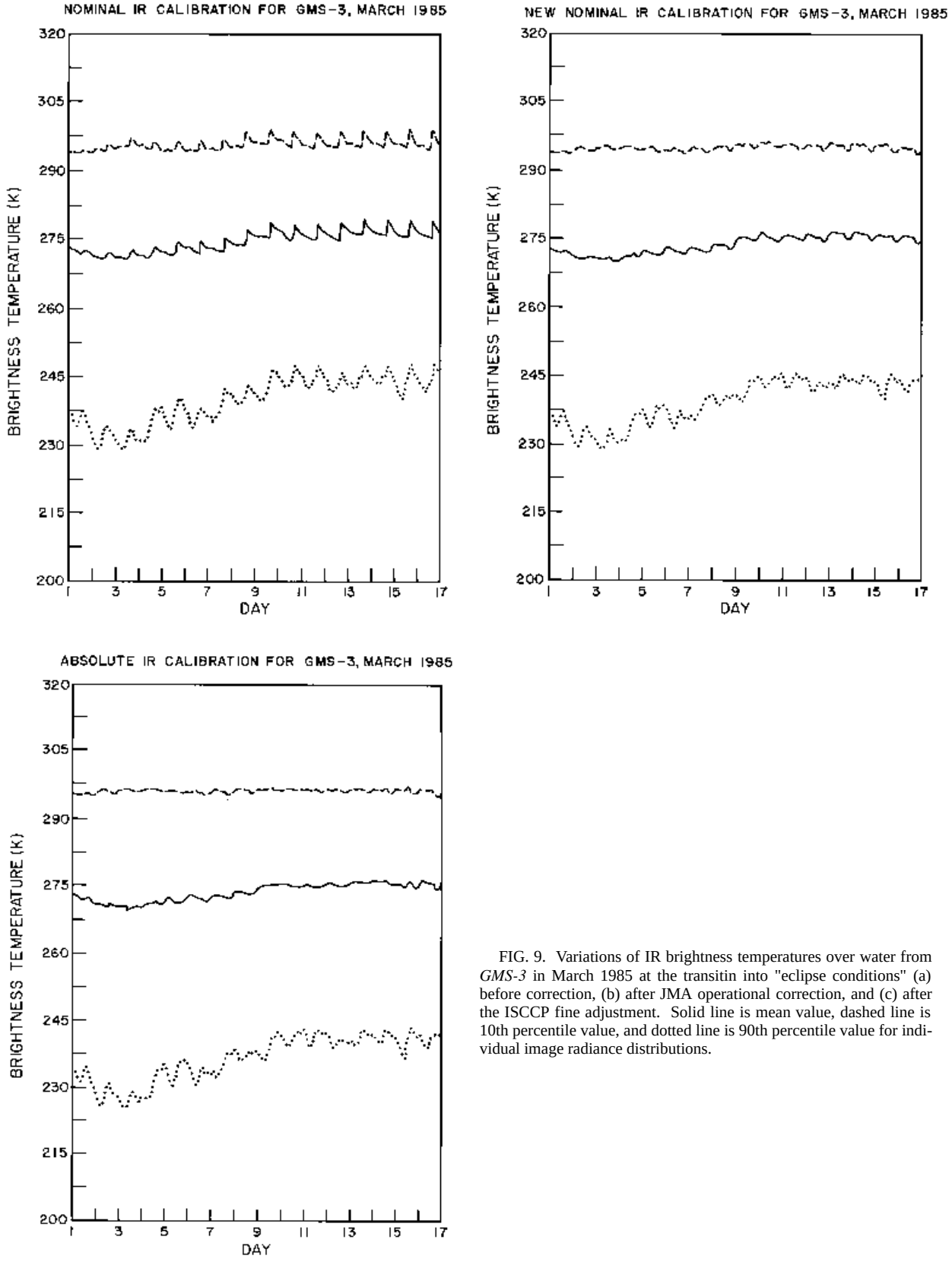

FIG. 9. Variations of IR brightness temperatures over water from *GMS-3* in March 1985 at the transitin into "eclipse conditions" (a) before correction, (b) after JMA operational correction, and (c) after the ISCCP fine adjustment. Solid line is mean value, dashed line is 10th percentile value, and dotted line is 90th percentile value for individual image radiance distributions.

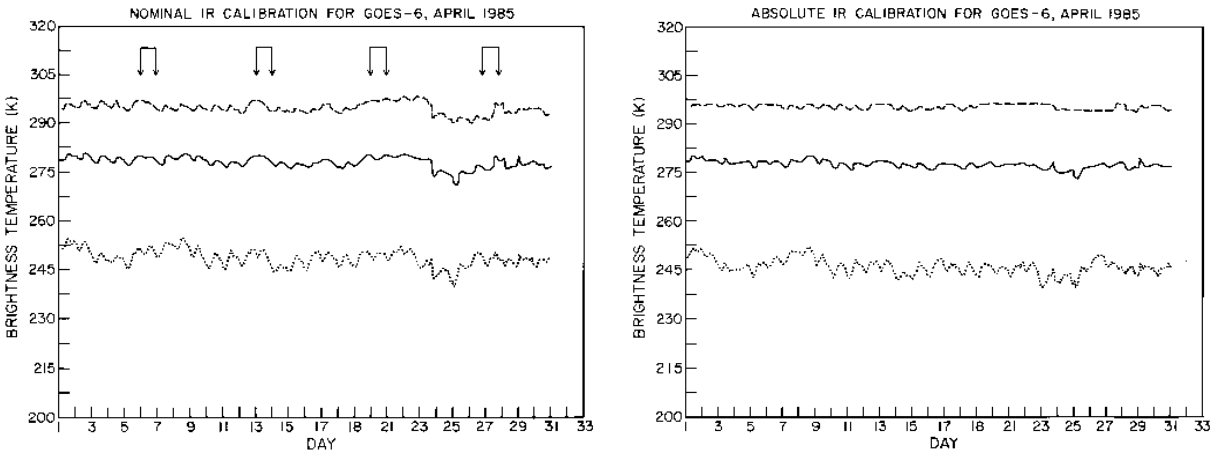

FIG. 10. Short-term variations of IR brightness temperatures from *GOES-6* for 1-30 April 1985: mean value (solid), 10th percentile (dashed), and 90th (dotted) percentile for individual image radiance distributions. Arrows indicate weekends. Original data are shown in (a) and corrected in (b).

in the lower percentile values), whereas the brighter VIS and colder IR statistics are associated with tropical and midlatitude cloud systems.

Figures 9, 10 and 11 show some examples of the kinds of short-term changes that have occurred. The most common problem is spurious diurnal variations in IR calibration, associated with changing temperatures in the instrument to the sun; this effect is exacerbated during eclipse[6] conditions twice a year.

2) DEFINITION OF LIMITS

Examination of the radiance distribution statistics for each satellite over several years provides an estimate of the lowest variability that occurs in the lower percentile values, which is interpreted to be real variations in ocean surface reflectance and temperature and the overlying atmosphere. We find that this variability is less than 2% for VIS and less than 1 K for IR; we use 2% for VIS and 1.5 K for IR as conservative limits. The variability of the higher percentile values, associated with clouds, is larger, but most spurious changes can be identified across the whole radiance distribution (cf., Figs. 9, 10, and 11). Most changes appear to be nearly constant offsets. Thus, this adjustment procedure is limited to determination of corrective offsets using the variations of the lower percentile values.

b. Adjustment procedure

1) IR RADIANCES

Short-term changes in the IR calibration are much more common than for VIS calibration. Particularly prevalent are spurious diurnal variations, which become most noticeable during the equinox seasons when the geostationary satellites go into Earth's shadow near local midnight and experience very large changes in temperature. Even in seasons where the satellites are illuminated continuously, the change in phasing of the solar illumination with orbital position can produce small temperature changes on the spacecraft. *Meteosat, GMS* and *GOES* are all spin-stabilized spacecraft, while *Insat* is three-axis stabilized. The new generation of *GOES* satellites will be three-axis stabilized. The former rotate very rapidly (usually 100 rpm), while the latter rotate very slowly (once per 24 h) with respect to the sun, producing very different heating environments. Each type of satellite has different strategies to deal with this variation in heating.

Meteosat operations actively compare the IR measurements with modeled radiances based on surface measurements of ocean temperature to remove spurious diurnal variations and provide fine gain adjustments for each image. Comparing solstice and equinox data from *Meteosat* shows little diurnal variation in the IR 10th percentile values during solstice, but a small 1-2-K diurnal variation during equinox. This result indicates that the *Meteosat* correction procedure is generally successful. Before 1989, JMA did not attempt to correct for such diurnal effects but began an active correction procedure in that year. Figure 9a shows equinox behavior before, and Fig. 9b after the introduction of a correction procedure. The 5-7 K diur

[6] Geostationary satellites orbit in the earth's equatorial plane, which is tilted with respect to the sun-earth plane except near equinoxes. At such times, but at no other, the satellite enters fully dark conditions near local midnight.

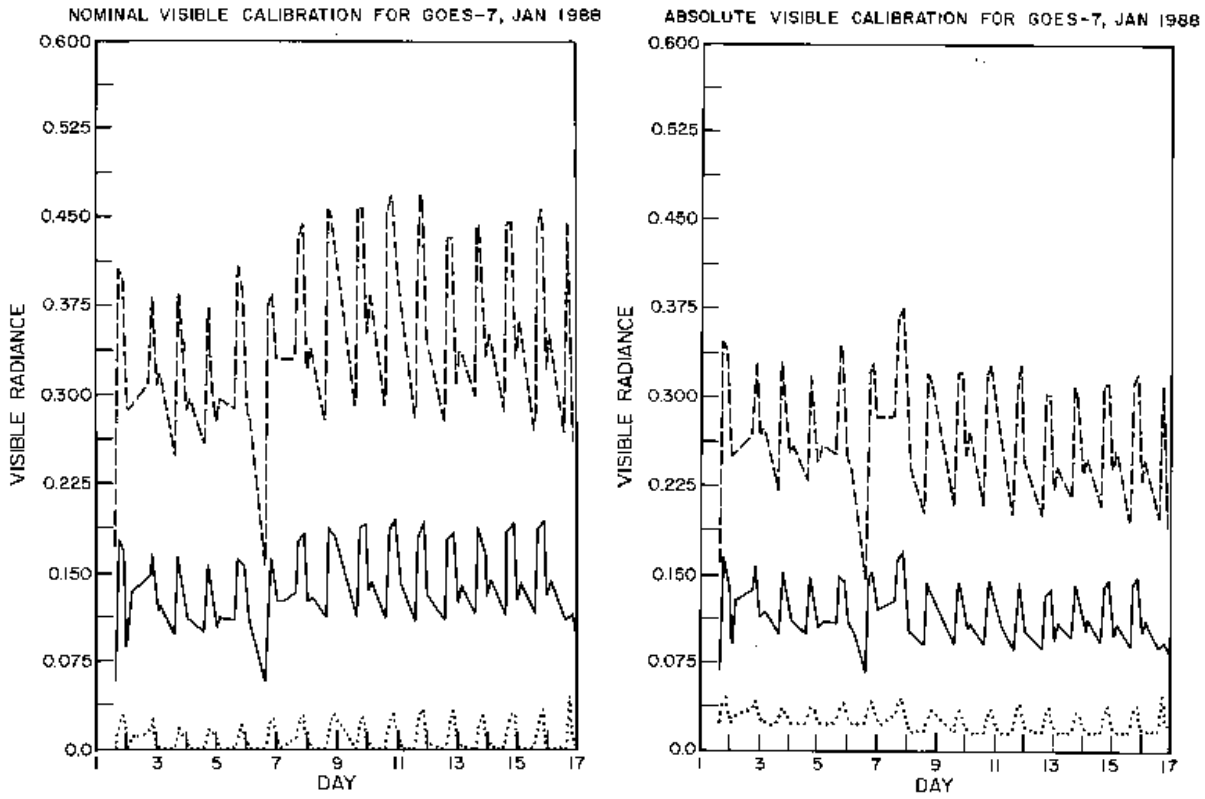

FIG. 11. Example of an anomalous variation of visible radiances interpreted to be due to a short-term change in calibration. Original data are represented in (a) by the mean value (solid) and the 10th (dashed) and 90th (dotted) percentile values from the distribution of radiances for individual images from *GOES-7* for 1-16 January 1988. Corrected data are shown in (b). The anomaly on day 7 is caused by partial images.

nal variation is reduced to 2-3 K. The results of our additional correction are shown in Fig. 9c. *GOES* satellites have on-board heaters that actively stabilize instrument temperatures. This approach is generally successful; however, when one of these heaters fails, as occurred on the *GOES-6* satellite in February 1984, diurnal variations of 3-5 K appear (Fig. 10a). In this case, routine satellite operations also called for switching a large IR sounder instrument off and on everyday, except on weekends, which altered instrument temperatures and produced quasi-diurnal variations in calibration. The corrected *GOES-6* radiances are shown in Fig. 10b.

The adjustment procedure applied to the IR data has four steps: 1) the image-by-image distributions of IR radiances are examined for biweekly periods, separated into land and ocean areas to identify any potential changes, 2) statistics describing the average distribution shape (10th percentile, mean, and 90th percentile values) are collected, 3) the same statistics are collected for the particular images used for normalizing the calibration to AVHRR, and 4) an allowed range of variation of the 10th percentile values (high temperatures) is calculated for each month of data.

The allowed range of 10th percentile values is determined by the average 10th percentile values for the normalization images, +0.5 K and - 1.0 K; however, the statistics over the entire time period between the normalization calculations (usually two months) are examined for consistency. The allowed range of 1.5 K is larger than the smallest diurnal variations observed in the 10th percentile values (which are usually less than 1.0 K). Moreover, the offset adjustments are calculated by the difference between the 10th percentile value for a particular image and the nearest boundary of the allowed range. Thus, this correction is conservative in allowing somewhat larger diurnal variability than observed and in correcting only to the edge of the allowed range, instead of forcing agreement with the average 10th percentile value. This approach insures that the data are not adjusted to a precision that is not justified, but sets a reasonable limit on the remaining uncertainties in the IR calibrations.

Figures 9c and 10b illustrate the effects of applying the method to the two illustrative cases. The rms magnitude and frequency of these corrections has been

Table 4. Corrections made to visible calibrations.

Satellite	Time period	Correction slope	Intercept
GMS-2	1 - 17 July 1984	2.420	0.000
GOES-7	1 - 7 January 1988	1.200	0.003
GOES-7	30 - 31 January 1988	0.825	-0.009
GOES-7	20 - 29 February 1988	1.240	0.004

about 0.7 K for about one-third of the *Meteosat* images, about 0.7 K for about 15% of *GOES* images (but about 1.2 K for about 35% of the images from *GOES-6*), and about 0.7 K for about 35% of *GMS* images.

2) VIS RADIANCES

Visible data are inspected in the same fashion, but most of the changes that could be reliably identified were already accommodated in changed normalization coefficients. Two exceptions have occurred: 1) *GMS-2* visible radiances appeared abnormally low during the first 17 days of July 1984, and 2) *GOES-7* visible radiances underwent several sudden transitions in late January through February 1988 (Fig. 11a). The first of these was caused by the inclusion of one failed visible channel in the average radiances; hence the necessary correction (Table 4) can be calculated from the fact that the average values should have been divided by three instead of four. The second event has not been explained. Using the bi-weekly average percentile statistics preceding and following the period shown in Fig. 11 and comparing them to the statistics in the anomalous periods, we calculate corrections (Table 4) to make the average radiance distributions the same (Fig. 11b). Since the distributions are very similar before and after this event, we assume that no significant changes in the tropical cloud properties have occurred.

The only other significant event was a change of gain by ESA for *Meteosat-2* on 12 May 1987, which was corrected by the normalization procedure.

5. Error assessment

Figures 5 and 6 summarize the magnitudes of the calibration changes being made: they are typically 3%-7% in VIS and 2-5 K in IR. Figures 10 and 11 show that sudden changes of this magnitude are readily discernable, but the main value of the ISCCP normalization procedure is to create a radiance dataset with a calibration that is uniform over the whole globe and over the whole time record (now planned to be at least 12 years). Calibration heterogeneity and variability, if uncorrected, precludes determination of larger spatial scale and longer time scale changes in cloud properties.

a. Residual differences

Overlapping observations by adjacent pairs of geostationary satellites can be compared to test the individual normalization results. A direct comparison of radiances (Fig. 12) shows that differences are less than 2% in visible and 2 K in IR. Recently, ESA has begun operating *Meteosat-3* at 50°W to improve satellite coverage of the Atlantic while only one *GOES* is available. Special datasets were to collected to compare the *Meteosat-3* and *Meteosat-4* calibrations. This direct comparison can also be used to check the normalization results, although the larger satellite zenith angles involved make the VIS comparison less reliable. For December 1991 and January 1992, the directly determined ratio of *Meteosat-3* to *Meteosat-4* calibration is 0.906 and 0.908 for VIS and 0.957 and 0.980 for IR.

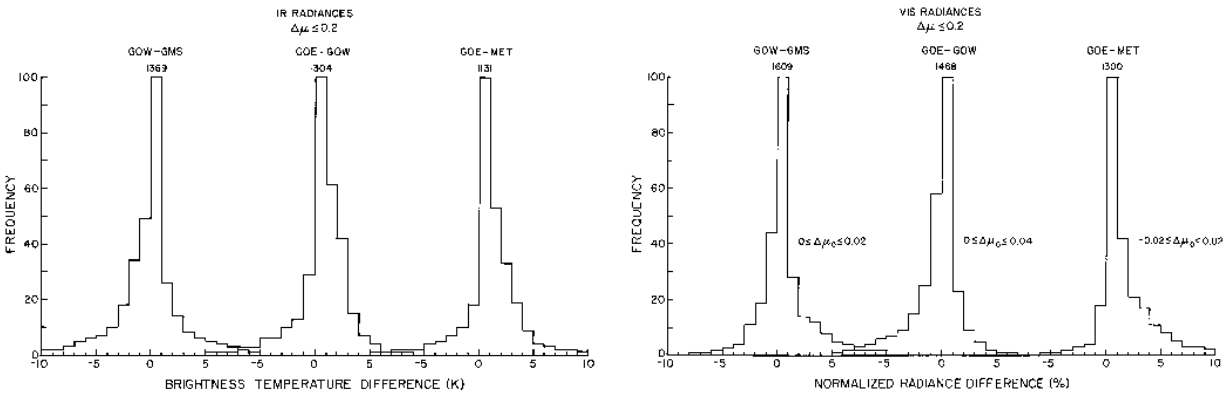

FIG. 12. Distributions of differences of (a) infrared and (b) visible radiances in overlapping regions between adjacent geostationary satellites. Coincident measurements are constrained to have the same values of the cosine of satellite zenith angle μ within 0.2 and the cosine of solar zenith angle μ_0 within the ranges shown. The total number of scenes meeting the criteria in 1 month of data (July 1983) are given at the peak of the histograms.

The corresponding ratios inferred from the separate normalizations to *NOAA-11* are 1.026 and 0.988 for VIS and 0.989 and 0.972 for IR. The VIS results agree to within approximately 10%, and the IR results within approximately 2%. The absolute calibration for *Meteosat-4* determined by ISCCP also appears consistent to ±10%, with results from a direct aircraft comparisons reported in the *Meteosat* calibration report (issue 9 for January-March 1991).

All of the ISCCP stage B3 data are analyzed by the GPC to produce the cloud climatology; as part of this analysis, the radiances are compared to radiative transfer model calculations to retrieve the physical properties of the surface and atmosphere. During the production of the monthly mean products (stage C2), all overlapping (collocated and nearly simultaneous) measurements of surface and cloud properties are compared for the whole month. Residual biases in these quantities provide another estimate of the uncertainty of the normalization procedures. Such comparisons over eight years of data indicate rms biases of 2%-3% in inferred visible reflectivities and about 1 K in inferred temperatures.

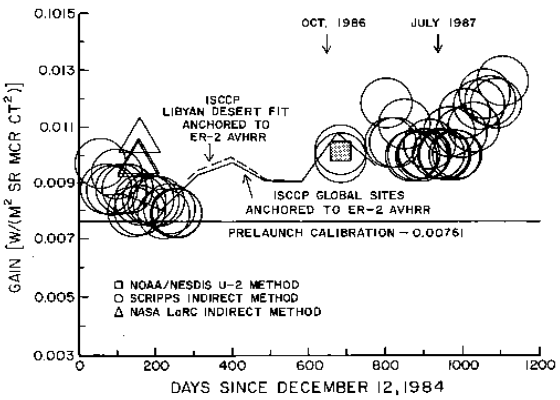

FIG. 13. Comparison of calibration gain corrections for *GOES-6* inferred from direct aircraft measurements, two indirect methods using White Sands, and the ISCCP normalization to the afternoon polar orbiter (from Whitlock et al. 1990a). The Scripps method calculates expected satellite measure-ments from a specified surface albedo. The ISCCP results are converted to an absolute calibration by comparing the *NOAA* calibration to aircraft data (ER-2 AVHRR); two different trend estimates are used (Libyan Desert and Global).

b. Confirmation of normalization of GOES

As part of an experiment to collect validation data for methods of calculating surface radiative fluxes using satellite radiance measurements, a special data collection effort, associated with the FIRE (First ISCCP Regional Experiment) cirrus intensive field observations during October 1986 in Wisconsin included a special effort to calibrate the satellite radiance measurements (Whitlock et al. 1990a). Not only did this effort provide one of the best calibrations of the visible channel on an AVHRR (cf. Brest and Rossow 1992), but it also provided an independent estimate of the normalization between *NOAA-9* and *GOES-6*. Figure 13, taken from Whitlock et al. (1990a), shows a comparison of the independent calibration of *GOES-6* with that inferred from *NOAA-9* by using the normalization determined by ISCCP. The solid line continues under the circles to the right but does not exceed 0.11. The agreement is excellent; the figure shows gain values where the disagreements are equivalent to differences in reflectances of less than 1%.

c. Indirect checks

Although indirect, attempts to calculate total radiation fluxes with the ISCCP stage B3 or stage C1 data can be compared with direct measurements of the same fluxes to reveal any serious biases in the calibrations. To date, such calculations (Whitlock et al. 1990b; Rossow et al. 1990; Bishop and Rossow 1992) have not indicated any biases greater than 7% in VIS and 2% in IR.

d. Error summary

Overall, uncertainties in the geostationary calibration come from the combination of uncertainties in the normalization and fine adjustments described here. The sensitivity tests of the normalization, together with the magnitudes of possible nonlinearities in the radiometers, suggest errors in the normalization of approximately 2% for VIS and 1.5 K for IR. The independent check of the *GOES-6* VIS calibration suggests a smaller estimate. The fine adjustment procedure generally involves small corrections to the IR, typically less than 1 K. The residual differences found in the processing of stage C2 data, together with indirect comparisons, suggest that the overall relative uncertainty in radiances may be about 3% in VIS and 1-2 K in IR. The largest uncertainty in *absolute* calibration comes from the absolute calibration of the polar orbiter. Comparing the remaining relative uncertainties to the magnitudes of changes made (Figs. 5 and 6) suggests that the ISCCP procedures have reduced the relative calibration uncertainties by at least a factor of 2.

Acknowledgments. Earlier versions of the normalization procedure at Centre Météorologie Spatiale were developed by Nicholas Beriot and Gerard Therry. Over the years the normalization analyses were performed by Claude Soulabail and Christian Bourdet. Analysis of *Insat* normalization at Colorado State University was performed by Kelly Dean. *Insat* data were provided to Colorado State University by Roy Jenne at

the National Center for Atmospheric Research. Collection of short-term calibration statistics at NASA Goddard Institute for Space Studies was performed by Mike Brown. Assistance in understanding satellite and instrument operations was given by Kathy Kidwell (*NOAA*, *NOAA* SPC), Brian Mason (ESA, *Meteosat* SPC), Frederick Mosher, Robert Fox and Don Wylie (University of Wisconsin, *GOES*-East SPC); Steve Lapczak, Francis Bowkett and Don McKay and Yves Durocher (AES, *GOES*-East SPC); and S. Kadowaki, Isao Kubota, Akio Kurosaki, Takenori Nuomi and Kenzo Shuto (JMA, *GMS* SPC). We also benefitted from discussions with K. Kriebel, R. Saunders, E. Raschke and M. Weinreb. We thank C. Koizumi for technical typing, and L. Del Valle for graphics.

APPENDIX

Calibration History

a. Nominal calibration

The nominal calibration represents the best information available at the start of processing of data from a particular satellite, usually the prelaunch calibration supplied by the satellite operator for the visible (VIS) channel and an equation or table used to interpret onboard calibration information for the infrared (IR) channel. The normalization results in part (b) are based on the following nominal calibrations [see Rossow et al. (1987) and Rossow et al. (1992) for complete details].

In this document, VIS radiances are given as "scaled radiances", L^*, defined as

$$L^* = \frac{\pi L}{E_O} \qquad \text{(A1)}$$

Here L^* is the scaled radiance expressed as a fraction from 0 to 1, where L is the radiance (W m^{-2} sr^{-1}) measured by the instrument, and E_O/π is the "solar constant" of the instrument representing the radiance that would be measured by the instrument when viewing a surface with unit (Lambertian) albedo illuminated by the (annual mean) sun.

The IR radiances are given as brightness temperatures TB representing the temperature of a blackbody that emits the same radiance in the radiometer bandpass, which are defined by:

$$L = \int_0^\infty \phi_\lambda \, B(\lambda, \mathrm{TB}) \, d\lambda, \qquad \text{(A2)}$$

where ϕ_λ is the spectral response of the radiometer and $B(\lambda, \mathrm{TB})$ is the Planck function.

1) *Meteosat* NOMINAL CALIBRATION

The calibration relations used for ISCCP for *Meteosat* satellites are

$$\textit{Meteosat-2}\ \ L^* = (3.641 \times 10^{-3})(\mathrm{CT}-2) \qquad \text{(A3a)}$$

$$\textit{Meteosat-3}\ \ L^* = (3.641 \times 10^{-3})(\mathrm{CT}-2) \qquad \text{(A3b)}$$

$$\textit{Meteosat-4}\ \ L^* = (3.641 \times 10^{-3})(\mathrm{CT}-2) \qquad \text{(A3c)}$$

where CT is an 8-bit count value. Original *Meteosat* VIS counts are 6-bit values.

Meteosat IR telemetry count values are converted to radiance units by

$$L_{IR} = f_{IR}\, G_{IR}\, (\mathrm{CT}-Y_{IR})\ (\mathrm{W\ m^{-2}\ sr^{-1}}), \qquad \text{(A4)}$$

where G_{IR} is the calibrated instrument gain, Y_{IR} the intercept, and f_{IR} the fine adjustment of gain factor. Parameters G_{IR} and Y_{IR} are determined from twice-daily measurements of earth and space by the radiometer; sample values are G_{IR} = 0.046 W m^{-2} sr^{-1} per count, and Y_{IR} = 5 counts. These values are held constant unless the mean bias between *Meteosat* observations and radiance calculations from ship measurements of SST exceeds ±0.5 K. Values of f_{IR} are calculated from measurements of the on-board calibration target; a typical value is 0.94. These values are reported for individual images.

The spectral response function of the IR channel, together with the Planck function of temperature, is used to relate radiances measured by this channel to blackbody temperatures; ESA documentation supplies a radiance-to-temperature conversion table. There is no simple relation between counts and temperatures. To make *Meteosat* IR data consistent with all other satellites, the count values in ISCCP B3 data have been changed to (255 - CT), so that high count values represent low radiances or brightness temperatures.

2) *GOES* NOMINAL CALIBRATION

Data from the eight separate VIS channels are processed to normalize the output from all the channels to a single reference channel. The reference channel for *GOES-5* is channel 8; for *GOES-6* is channel 2, and for *GOES-7* is channel 1. In ISCCP radiance data the outputs of the eight detectors is averaged to produce a single, lower resolution radiance measurement, which is treated as equivalent to measurements by the reference channel.

The conversion of telemetry count values to radiance uses the following relations:

$$\textit{GOES-5}\ \ L^* = (2.170 \times 10^{-5})(\mathrm{CT}^2 - 0.016) \qquad \text{(A5a)}$$

$$\textit{GOES-6}\ \ L^* = (2.121 \times 10^{-5})(\mathrm{CT}^2 - 0.016) \qquad \text{(A5b)}$$

$$\textit{GOES-7}\ \ L^* = (1.855 \times 10^{-5})(\mathrm{CT}^2 - 0.016) \qquad \text{(A5c)}$$

where CT is an 8-bit count value. Original *GOES* VIS counts are 6-bit values.

A processing error has been discovered in the Stage B3 data for *GOES-5* and *GOES-6* from July 1983 through May 1984 that is equivalent to adding 0.5 W m^{-2} sr^{-1} to all nominal VIS radiances or about 0.5% to

scaled radiances. Since this error is well within the uncertainty of the calibration, no correction was made.

Calibration of the IR channel is performed once per week using an on-board blackbody source that is viewed by the detector directly. The results of the on-board calibration sequence are used to calculate tables relating telemetry count values to blackbody temperatures. The blackbody temperatures are related to the radiances by integrating the Planck function times the spectral response function. Application of the calibration tables produces count values transmitted to users that are related to blackbody temperatures by a fixed relationship:

$$\text{TB} = 330 - \text{CT}/2, \text{ for } 0 \le \text{CT} < 176$$

$$\text{TB} = 418 - \text{CT}, \text{ for } 176 \le \text{CT} < 255 \qquad \text{(A6)}$$

Radiances are obtained from these temperatures using the calculated relationship between brightness temperatures and radiances.

In April 1987 *NOAA* changed the telemetry format for *GOES* data which increased the number of bits used to record VIS radiances from 6 to 8 and IR radiances from 8 to 10. In the ISCCP data processing, the extra IR radiance resolution was exploited to produce an 8 bit representation (produced by G.G. Campbell), with count values nearly linear in radiance rather than linear in brightness temperature as before (Rossow et al. 1992). This change made *GOES* IR data more like data from all other satellites; however, no simple formula relates ISCCP count values with temperatures.

Short time scale variations in the calibration, particularly those associated with diurnal heating-cooling cycles of the satellite, are not monitored for *GOES*.

3) *GMS* NOMINAL CALIBRATION

GMS VIS data represent an average over (usually) four detectors, after normalization to a reference channel (channel 7 on *GMS-1*, channel 1 on *GMS-2*, channel 5 on *GMS-3* and channel 3 on *GMS-4*). The calibration coefficients for the reference channel are fixed based on a combination of prelaunch and postlaunch measurements. Solar channel data for ISCCP represent an average of the measurements from channels 5, 7 and 8 for *GMS-1*, channels 1-4 for *GMS-2*, channels 5-8 for *GMS-3*, and channels 1-4 for *GMS-4*. The calibration coefficients are used to convert the original 6 bit count values to scaled radiances, which are then averaged and rescaled to an 8-bit count scale in ISCCP data using

$$L^* = \left(\frac{\text{CT}}{255}\right)^2 \qquad \text{(A7)}$$

For the infrared the results of daily (now eight times daily) calibration observations are used to produce a table relating 8 bit count values to blackbody temperatures; these tables are provided with the data. In operation, the backup IR channel is used on *GMS-1* and the primary channel is used on *GMS-2, GMS-3* and *GMS-4*. There is no simple relation between count values and temperatures.

Shorter period variations in calibration due to the diurnal heating-cooling cycle were not monitored for the *GMS* satellites prior to March 1987.

4) *INSAT* NOMINAL CALIBRATION

Insat VIS data represent a sample from one of four sensors; the original spatial resolution is 2.75 km, which is reduced to a spacing of about 22 km. No information is available about which set of sensors is operational or about whether the sampling provides data consistently from one particular sensor. No nominal calibration is available for *Insat* VIS data. Thus, the spectral response is assumed to be the average over the primary set of VIS sensors, and the nominal calibration is arbitrarily set to

$$L^* = 0.004\text{CT}, \qquad \text{(A8)}$$

where CT is an 8-bit count value. The original *Insat* VIS data are reported as 6-bit count values.

On-board calibration of IR radiances is used to convert to standard 8-bit count values; the frequency of calibration is not known. The standard IR count values are related to brightness temperatures by a fixed relationship:

$$\text{TB} = \begin{cases} 179 + (255 - \text{CT}), & 150 \le \text{CT} \le 253 \\ 284 + 0.127\,(150 - \text{CT}), & 16 < \text{CT} < 150 \\ 301 + (16 - \text{CT}), & 0 \le \text{CT} \le 16 \end{cases} \qquad \text{(A9)}$$

b. History of normalization coefficients

Tables A1, A2 and A3 give the history of the normalization coefficients for *Meteosat, GOES* and *GMS*. Table 3 gives the same information for *Insat*. Note that these values have been modified to correct for any changes in the AVHRR calibration (cf. Brest and Rossow 1992).

Final calibrations (without short-term corrections) are obtained by using the coefficients in Tables A1, A2 and A3 to alter the nominal values:

$$\text{for visible } L_A^* = 1.2 \text{ x slope x } L_N^* + \text{interc} \qquad \text{(A10)}$$

$$\text{for infrared } T_A = \text{slope x } T_N + \text{interc} \qquad \text{(A11)}$$

where L_A^* and L_N^* are the absolute and nominal visible scaled radiances and T_A and T_N are the absolute and nominal brightness temperatures, respectively.

Table A1. History of visible and infrared normalization coefficients for Meteosat.

	Visible (fraction)		Infrared (K)			Visible (fraction)		Infrared (K)	
Month	Slope	Intercept	Slope	Intercept	Month	Slope	Intercept	Slope	Intercept
					Meteosat-2				
July 1983	1.068	0.000	1.030	-9.47	May 1984	1.017	-0.001	1.074	-20.20
August 1983	1.070	0.001	1.044	-13.33	June 1984	1.024	0.003	1.075	-20.85
September 1983	1.073	0.001	1.058	-17.19	July 1984	1.030	0.006	1.075	-21.50
October 1983	1.075	0.002	1.072	-21.05	August 1984	1.033	0.003	1.080	-22.89
November 1983	1.046	0.004	1.054	-16.06	September 1984	1.037	0.001	1.085	-24.27
December 1983	1.016	0.006	1.037	-11.07	October 1984	1.040	-0.002	1.090	-25.66
January 1984	0.997	0.007	1.025	-7.83	November 1984	1.031	-0.001	1.075	-21.06
February 1984	1.002	0.003	1.041	-11.74	December 1984	1.022	0.001	1.060	-16.46
March 1984	1.006	0.000	1.058	-15.64	January 1985	1.013	0.002	1.045	-11.86
April 1984	1.011	-0.004	1.074	-19.55					
					change from *NOAA-7* to *NOAA-9* as normalization standard				
February 1985	1.093	0.004	1.101	-29.60	April 1986	0.977	0.007	1.104	-29.50
March 1985	1.042	0.005	1.094	-27.00	May 1986	0.983	0.009	1.105	-29.90
April 1985	0.991	0.005	1.086	-24.40	June 1986	0.987	0.011	1.105	-30.30
May 1985	0.989	0.005	1.080	-22.83	July 1986	0.991	0.013	1.106	-30.70
June 1985	0.990	0.005	1.074	-21.27	August 1986	1.004	0.008	1.101	-29.30
July 1985	0.987	0.005	1.068	-19.70	September 1986	1.018	0.004	1.096	-27.90
August 1985	0.983	0.005	1.057	-16.87	October 1986	1.033	-0.001	1.051	-14.87
September 1985	0.980	0.006	1.047	-14.03	November 1986	1.014	0.000	1.114	-32.50
October 1985	0.975	0.007	1.036	-11.20	December 1986	0.995	0.001	1.096	-27.05
November 1985	0.964	0.009	1.046	-13.53	January 1987	0.977	0.002	1.079	-21.60
December 1985	0.952	0.010	1.055	-15.87	February 1987	0.983	0.003	1.082	-22.80
January 1986	0.939	0.012	1.065	-18.20	March 1987	0.988	0.005	1.084	-24.00
February 1986	0.952	0.010	1.078	-21.97	April 1987	0.995	0.006	1.087	-25.20
March 1986	0.964	0.009	1.091	-25.73					
					gain change in VIS channel on *Meteosat-2*				
May 1987	0.835	0.004	1.100	-28.63	January 1988	0.835	0.003	1.090	-24.27
June 1987	0.842	0.003	1.112	-32.07	February 1988	0.822	0.002	1.089	-24.41
July 1987	0.849	0.002	1.125	-35.50	March 1988	0.808	0.002	1.088	-24.55
August 1987	0.839	0.004	1.110	-31.13	April 1988	0.795	0.001	1.087	-24.69
September 1987	0.829	0.005	1.096	-26.77	May 1988	0.781	0.001	1.086	-24.83
October 1987	0.820	0.007	1.122	-34.75	June 1988	0.768	0.000	1.085	-24.97
November 1987	0.824	0.006	1.112	-31.25	July 1988	0.771	0.000	1.085	-24.97
December 1987	0.830	0.004	1.100	-27.77	August 1988	0.774	0.000	1.085	-24.97
					Meteosat-3				
August 1988	0.817	-0.019	1.054	-16.38	October 1988	0.869	-0.021	1.081	-21.67
September 1988	0.842	-0.019	1.067	-19.03					
					change from *NOAA-9* to *NOAA-11* as normalization standard				
November 1988	0.796	-0.006	1.085	-22.53	January 1990	0.905	-0.001	1.089	-23.57
December 1988	0.782	-0.005	1.089	-23.79	February 1990	0.905	-0.001	1.089	-23.57
January 1989	0.767	-0.005	1.094	-25.05	March 1990	0.904	-0.005	1.088	-23.67
February 1989	0.771	-0.005	1.095	-24.69	April 1990	0.903	-0.007	1.086	-23.78
March 1989	0.774	-0.006	1.095	-24.32	October 1990	0.903	-0.007	1.086	-23.78
April 1989	0.774	-0.006	1.095	-24.32	November 1990	0.903	-0.007	1.086	-23.78
May 1989	0.774	-0.006	1.095	-24.32	December 1990	0.903	-0.007	1.086	-23.78
June 1989	0.761	-0.002	1.085	-22.88					
					Meteosat-4				
June 1989	0.842	-0.027	1.090	-23.69	August 1990	0.856	-0.018	1.072	-19.37
July 1989	0.818	-0.013	1.092	-25.17	September 1990	0.879	-0.018	1.077	-20.60
August 1989	0.838	-0.015	1.092	-24.73	October 1990	0.901	-0.019	1.081	-21.82
September 1989	0.858	-0.016	1.090	-24.30	November 1990	0.888	-0.015	1.082	-22.48
October 1989	0.879	-0.018	1.090	-23.87	December 1990	0.874	-0.011	1.083	-23.13
November 1989	0.862	-0.016	1.090	-24.13	January 1991	0.860	-0.008	1.072	-19.87
December 1989	0.845	-0.014	1.092	-24.41	February 1991	0.764	-0.010	1.079	-21.51
January 1990	0.828	-0.012	1.092	-24.68	March 1991	0.866	-0.013	1.084	-23.13
April 1990	0.859	-0.015	1.093	-24.79	April 1991	0.868	-0.016	1.090	-24.76
May 1990	0.854	-0.015	1.093	-24.79	May 1991	0.853	-0.015	1.084	-23.28
June 1990	0.843	-0.016	1.078	-21.42	June 1991	0.836	-0.015	1.079	-21.78
July 1990	0.834	-0.017	1.068	-18.16					

TABLE A2. History of visible and infrared normalization coefficients for ***GOES***.

Month	Visible (fraction) Slope	Visible (fraction) Intercept	Infrared (K) Slope	Infrared (K) Intercept	Month	Visible (fraction) Slope	Visible (fraction) Intercept	Infrared (K) Slope	Infrared (K) Intercept
				GOES-5					
July 1983	0.665	-0.004	1.117	-30.92	February 1984	0.580	0.009	1.066	-18.81
August 1983	0.653	0.000	1.111	-29.33	March 1984	0.600	0.007	1.078	-22.08
September 1983	0.642	0.005	1.104	-27.74	April 1984	0.620	0.006	1.089	-25.34
October 1983	0.630	0.009	1.098	-26.15	May 1984	0.625	0.006	1.102	-28.24
November 1983	0.607	0.009	1.084	-22.62	June 1984	0.631	0.006	1.116	-31.14
December 1983	0.583	0.009	1.069	-19.08	July 1984	0.636	0.006	1.129	-34.04
January 1984	0.560	0.010	1.055	-15.55					
				GOES-6					
July 1983	0.675	-0.001	1.034	-9.20	May 1984	0.668	0.011	1.057	-15.43
August 1983	0.685	-0.004	1.041	-11.43	June 1984	0.645	0.011	1.059	-15.37
September 1983	0.694	-0.007	1.049	-13.67	July 1984	0.623	0.012	1.060	-15.30
October 1983	0.704	-0.010	1.056	-15.90	August 1984	0.645	0.011	1.061	-15.67
November 1983	0.708	-0.004	1.059	-16.33	September 1984	0.697	0.010	1.061	-16.03
December 1983	0.713	0.002	1.061	-16.77	October 1984	0.750	0.009	1.062	-16.40
January 1984	0.717	0.008	1.064	-17.20	November 1984	0.737	0.008	1.037	-10.20
February 1984	0.708	0.009	1.061	-16.63	December 1984	0.724	0.007	1.012	-4.00
March 1984	0.699	0.009	1.059	-16.07	January 1985	0.724	0.007	1.012	-4.00
April 1984	0.690	0.010	1.056	-15.50					
				change from *NOAA-7* to *NOAA-9* as normalization standard					
February 1985	0.649	0.008	1.046	-14.70	March 1986	0.711	0.006	1.078	-22.03
March 1985	0.651	0.008	1.046	-14.70	April 1986	0.692	0.007	1.077	-22.40
April 1985	0.677	0.005	1.070	-19.90	May 1986	0.678	0.009	1.074	-20.93
May 1985	0.662	0.007	1.076	-21.23	June 1986	0.664	0.012	1.070	-19.47
June 1985	0.646	0.009	1.083	-22.57	July 1986	0.649	0.014	1.067	-18.00
July 1985	0.630	0.010	1.089	-23.90	August 1986	0.691	0.011	1.054	-13.83
August 1985	0.660	0.010	1.091	-24.47	September 1986	0.733	0.009	1.040	-9.67
September 1985	0.691	0.008	1.093	-25.03	October 1986	0.776	0.006	1.056	-14.15
October 1985	0.721	0.007	1.095	-25.60	November 1986	0.748	0.010	1.052	-12.90
November 1985	0.731	0.005	1.088	-23.45	December 1986	0.720	0.013	1.077	-20.30
December 1985	0.741	0.005	1.080	-21.30	January 1987	0.692	0.017	1.102	-27.70
January 1986	0.751	0.003	1.080	-21.30	February 1987	0.674	0.013	1.100	-28.60
February 1986	0.732	0.005	1.079	-21.67	March 1987	0.655	0.008	1.098	-29.50
				change to AAA format on *GOES*—new IR calibration coding introduced					
April 1987	0.669	0.009	1.112	-33.17	February 1988	0.717	0.012	1.073	-21.29
May 1987	0.682	0.010	1.125	-36.83	March 1988	0.666	0.012	1.068	-19.98
June 1987	0.695	0.011	1.139	-40.50	April 1988	0.615	0.013	1.064	-18.66
July 1987	0.710	0.019	1.119	-33.90	May 1988	0.612	0.014	1.065	-18.94
August 1987	0.734	0.017	1.106	-30.10	June 1988	0.611	0.016	1.067	-19.21
September 1987	0.758	0.015	1.093	-26.30	July 1988	0.609	0.017	1.068	-19.49
October 1987	0.783	0.013	1.121	-34.86	August 1988	0.625	0.015	1.077	-22.26
November 1987	0.778	0.012	1.107	-30.78	September 1988	0.642	0.014	1.088	-25.03
December 1987	0.772	0.012	1.092	-26.69	October 1988	0.659	0.012	1.097	-27.80
January 1988	0.768	0.011	1.077	-22.61					
				change from *NOAA-9* to *NOAA-11* as normalization standard					
November 1988	0.650	-0.011	1.089	-25.30	January 1989	0.656	0.009	1.076	-21.67
December 1988	0.653	0.010	1.082	-23.48					
				GOES-7					
April 1987	0.543	0.013	1.131	-34.94					
				trend present in April—change at 13th					
April 1987	0.666	0.016	1.131	-34.94	February 1988	0.549	0.026	1.087	-24.57
May 1987	0.668	0.016	1.131	-34.94	March 1988	0.683	0.009	1.090	-24.72
June 1987	0.673	0.016	1.126	-34.21	April 1988	0.706	0.017	1.092	-24.89
July 1987	0.678	0.016	1.122	-33.48	May 1988	0.708	0.016	1.099	-27.33
August 1987	0.707	0.022	1.097	-26.30	June 1988	0.703	0.024	1.107	-29.77
September 1987	0.734	0.029	1.071	-19.13	July 1988	0.696	0.032	1.037	-10.46
October 1987	0.764	0.036	1.086	-23.90	August 1988	0.733	0.030	1.096	-26.76
November 1987	0.778	0.028	1.086	-24.26	September 1988	0.769	0.029	1.097	-26.91
December 1987	0.793	0.021	1.087	-24.57	October 1988	0.808	0.027	1.098	-27.07
January 1988	0.663	0.015	1.087	-24.57					
				change from *NOAA-9* to *NOAA-11* as normalization standard					
November 1988	0.704	0.024	1.060	-16.55	December 1988	0.704	0.024	1.060	-16.55

TABLE A2. *(Continued)*

Month	Visible (fraction) Slope	Visible (fraction) Intercept	Infrared (K) Slope	Infrared (K) Intercept	Month	Visible (fraction) Slope	Visible (fraction) Intercept	Infrared (K) Slope	Infrared (K) Intercept
				change to new AAA IR calibration coding					
January 1989	0.687	0.012	1.092	-25.51	April 1990	0.734	0.008	1.079	-21.45
February 1989	0.710	0.013	1.070	-19.75	May 1990	0.724	0.011	1.085	-23.16
March 1989	0.709	0.013	1.076	-20.81	June 1990	0.717	0.014	1.090	-24.94
April 1989	0.707	0.013	1.080	-21.88	July 1990	0.709	0.017	1.097	-26.68
May 1989	0.697	0.012	1.088	-24.55	August 1990	0.690	0.019	1.088	-23.91
June 1989	0.688	0.012	1.098	-27.22	September 1990	0.719	0.025	1.081	-21.99
July 1989	0.680	0.011	1.106	-29.88	October 1990	0.772	0.022	1.087	-24.44
August 1989	0.700	0.012	1.102	-28.60	November 1990	0.790	0.019	1.078	-21.93
September 1989	0.721	0.013	1.098	-27.32	December 1990	0.807	0.015	1.068	-19.43
October 1989	0.742	0.014	1.083	-22.64	January 1991	0.819	0.019	1.083	-23.59
November 1989	0.744	0.016	1.071	-19.29	February 1991	0.757	0.017	1.066	-18.36
December 1989	0.746	0.017	1.059	-15.95	March 1991	0.755	0.020	1.105	-29.24
January 1990	0.749	0.019	1.056	-22.09	April 1991	0.743	0.016	1.092	-25.51
February 1990	0.746	0.015	1.064	-17.75	May 1991	0.748	0.018	1.082	-22.09
March 1990	0.740	0.012	1.071	-19.61	June 1991	0.721	0.023	1.077	-20.60

TABLE A3. History of visible and infrared normalization coefficients for GMS.

Month	Visible (fraction) Slope	Visible (fraction) Intercept	Infrared (K) Slope	Infrared (K) Intercept	Month	Visible (fraction) Slope	Visible (fraction) Intercept	Infrared (K) Slope	Infrared (K) Intercept
					GMS-1				
January 1984	1.328	-0.003	1.046	-11.38	April 1984	1.334	-0.004	1.035	-8.44
February 1984	1.328	-0.003	1.046	-11.38	May 1984	1.334	-0.004	1.035	-8.44
March 1984	1.341	-0.004	1.040	-10.08	June 1984	1.334	-0.004	1.035	-8.84
					GMS-2				
July 1983	1.132	0.012	1.036	-8.25	January 1984	1.121	0.013	1.015	-4.53
August 1983	1.119	0.017	1.032	-7.74					
September 1983	1.106	0.021	1.027	-7.24	July 1984	0.909	-0.014	1.058	-14.20
October 1983	1.093	0.026	1.023	-6.73	August 1984	0.909	-0.014	1.058	-14.20
November 1983	1.102	0.022	1.020	-6.00	September 1984	0.895	-0.015	1.058	-15.66
December 1983	1.112	0.017	1.018	-5.26					
					GMS-3				
September 1984	0.991	-0.014	1.049	-12.90	December 1984	1.016	-0.020	1.047	-11.90
October 1984	0.991	-0.014	1.049	-12.90	January 1985	1.028	-0.023	1.046	-11.40
November 1984	1.003	-0.017	1.048	-12.40					
					change from *NOAA-7* to *NOAA-9* as normalization standard				
February 1985	0.876	0.000	1.068	-19.50	January 1987	0.972	0.002	1.073	-19.92
March 1985	0.907	-0.003	1.070	-19.15	February 1987	0.982	0.002	1.072	-19.65
April 1985	0.937	-0.006	1.071	-18.80	March 1987	0.994	0.002	1.071	-19.37
May 1985	0.928	-0.005	1.079	-20.98	April 1987	1.005	0.002	1.070	-19.10
June 1985	0.918	-0.005	1.088	-23.17	May 1987	1.004	0.003	1.075	-20.10
July 1985	0.908	-0.004	1.096	-25.35	June 1987	1.002	0.003	1.079	-21.10
August 1985	0.920	-0.001	1.088	-23.39	July 1987	1.001	0.004	1.084	-22.10
September 1985	0.933	0.001	1.080	-21.44	August 1987	1.033	0.000	1.080	-21.62
October 1985	0.945	0.004	1.072	-19.48	September 1987	1.066	-0.003	1.076	-21.15
November 1985	0.943	0.003	1.073	-19.92	October 1987	1.099	-0.006	1.060	-16.79
December 1985	0.941	0.001	1.075	-20.36	November 1987	1.085	-0.006	1.051	-14.23
January 1986	0.939	0.000	1.076	-20.80	December 1987	1.070	-0.004	1.050	-13.96
February 1986	0.937	-0.001	1.076	-20.66	January 1988	1.057	-0.003	1.046	-12.75
March 1986	0.935	-0.002	1.077	-20.52	February 1988	1.082	-0.007	1.049	-13.22
April 1986	0.934	-0.002	1.077	-20.38	March 1988	1.108	-0.010	1.051	-13.69
May 1986	0.935	-0.002	1.079	-20.70	April 1988	1.134	-0.014	1.055	-14.17
June 1986	0.934	-0.002	1.082	-21.02	May 1988	1.141	-0.014	1.055	-14.15
July 1986	0.933	-0.002	1.084	-21.34	June 1988	1.147	-0.014	1.056	-14.12
August 1986	0.965	-0.002	1.061	-15.37	July 1988	1.155	0.014	1.056	-14.10
September 1986	0.996	-0.002	1.038	-9.39	August 1988	1.140	-0.015	1.056	-14.38
October 1986	1.029	-0.003	1.043	-12.02	September 1988	1.125	-0.014	1.055	-14.65
November 1986	1.010	-0.002	1.034	-8.92	October 1988	1.111	-0.014	1.055	-14.93
December 1986	0.990	0.000	1.054	-14.42					

TABLE A3. *(Continued)*

Month	Visible (fraction) Slope	Visible (fraction) Intercept	Infrared (K) Slope	Infrared (K) Intercept	Month	Visible (fraction) Slope	Visible (fraction) Intercept	Infrared (K) Slope	Infrared (K) Intercept
change from *NOAA-9* to *NOAA-11* as normalization standard									
November 1988	1.047	0.000	1.063	-16.97	June 1989	1.019	0.001	1.073	-18.82
December 1988	1.026	0.004	1.058	-15.85	July 1989	1.019	-0.002	1.074	-18.83
January 1989	1.004	0.008	1.053	-14.73	August 1989	1.030	0.001	1.071	-18.42
February 1989	1.009	0.007	1.060	-16.09	September 1989	1.041	0.003	1.069	-18.02
March 1989	1.014	0.007	1.066	-17.45	October 1989	1.052	0.006	1.056	-14.29
April 1989	1.019	0.006	1.072	-18.81	November 1989	1.063	0.004	1.058	-15.55
May 1989	1.019	0.003	1.073	-18.82					
					GMS-4				
December 1989	0.838	-0.004	1.054	-14.60	October 1990	0.960	0.002	1.067	-18.47
January 1990	0.831	0.000	1.073	-20.17	November 1990	0.960	0.001	1.064	-17.77
February 1990	0.870	-0.005	1.071	-19.57	December 1990	0.959	0.001	1.061	-17.08
March 1990	0.885	-0.003	1.068	-18.97	January 1991	0.958	0.000	1.057	-16.23
April 1990	0.922	-0.001	1.066	-18.36	February 1991	0.961	0.000	1.060	-16.58
May 1990	0.907	0.001	1.065	-17.75	March 1991	0.961	-0.001	1.062	-16.94
June 1990	0.894	0.004	1.065	-17.15	April 1991	0.963	-0.001	1.064	-17.29
July 1990	0.882	0.006	1.064	-16.55	May 1991	0.959	-0.001	1.067	-17.72
August 1990	0.908	0.005	1.065	-17.19	June 1991	0.952	0.000	1.069	-18.15
September 1990	0.934	0.003	1.066	-17.83					

REFERENCES

Bishop, J. K. B., and W. B. Rossow, 1991: Spatial and temporal variability of global surface solar irradiance. *J. Geophys. Res.*, **96**, 16 839-16 858.

Brest, C. L. and W. B. Rossow, 1992: Radiometric calibration and monitoring of ***NOAA*** AVHRR data for ISCCP. *Int. J. Remote Sens*., **13**, 235-273.

Rossow, W. B., and R. A. Schiffer, 1991: ISCCP cloud data products. *Bull. Amer. Meteor. Soc*., **72**, 2-20.

——, Y. Zhang, and A. A. Lacis, 1990: Calculations of atmospheric radiative flux profiles. *Proc. of the AMS Seventh Conf. On Atmospheric Radiation*, San Francisco, Amer. Meteor. Soc., 81-86

——,E. Kinsella, A. Wolf, and L. Garder, 1987: International Satellite Cloud Climatology Project (ISCCP) description of reduced resolution radiance data. WMO/TD No. 58. (revised), World Climate Research Program, Geneva, 143 pp.

——,Y. Desormeaux, C. L. Brest, and A. W. Walker, 1992: International Satellite Cloud Climatology Project (ISCCP) Radiance Calibration Report. WMO/TD No. 520, World Climate Research Program, Geneva 104 pp.

Schiffer, R. A., and W. B. Rossow, 1983: The International Satellite Cloud Climatology Project (ISCCP): The first project of the World Climate Research Program. *Bull. Amer. Meteor. Soc*., **64**, 779-784.

——, and ——, 1985: ISCCP global radiance data set: A new resource for climate research. *Bull. Amer. Meteor. Soc*., **66**, 1498-1505.

Sèze, G., and W. B. Rossow, 1991: Time-cumulated visible an infrared radiance histograms used as a descriptor of surface and cloud variations. *Int. J. Remote Sens*., **12,** 877-920.

Whitlock, C. H., W. F. Staylor, G. Smith, R. Levin, R. Frouin, C. Gautier, P. M. Teillet, P. N. Slater, Y. J. Kaufman, B. N. Holben, W. B. Rossow, C. L. Brest, and S. R. LeCroy, 1990a: AVHRR and VISSR satellite instrument calibration results for both cirrus and marine stratocumulus IFO periods. FIRE Science Report 1988. NASA CP-3083, 141-145.

——, ——,W. L. Darnell, M. D. Chou, G. Dedieu, P. Y. Deschamps, J. Ellis, C. Gautier, R. Frouin, R. T. Pinker, I. Laslo, W. B. Rossow, and D. Tarpley, 1990b: Comparison of surface radiation budget satellite algorithms for downwelled shortwave irradiance with Wisconsin FIRE/SRB surface-truth data. *Seventh Conf. on Atmospheric Radiation*, San Francisco, Amer. Meteor. Soc., 64-67.